

**UNCLASSIFIED**

**AD 4 2 3 9 8 3**

**DEFENSE DOCUMENTATION CENTER**

**FOR**

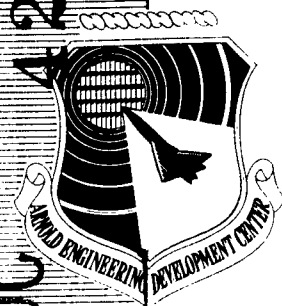
**SCIENTIFIC AND TECHNICAL INFORMATION**

**CAMERON STATION, ALEXANDRIA, VIRGINIA**



**UNCLASSIFIED**

423983



# **GASDYNAMIC DIAGNOSIS OF HIGH-SPEED FLOWS EXPANDED FROM PLASMA STATES**

**By**

**J. Leith Potter, George D. Arney, Jr.,  
Max Kinslow, and William H. Carden  
von Kármán Gas Dynamics Facility  
ARO, Inc.**

**TECHNICAL DOCUMENTARY REPORT NO. AEDC-TDR-63-241**

**November 1963**

**Program Element 62405334/8950, Task 895004**

**(Prepared under Contract No. AF 40(600)-1000 by ARO, Inc.,  
contract operator of AEDC, Arnold Air Force Station, Tenn.)**

**ARNOLD ENGINEERING DEVELOPMENT CENTER  
AIR FORCE SYSTEMS COMMAND  
UNITED STATES AIR FORCE**

CATALOGED BY DDC  
AS AD NO.

# ***NOTICES***

Qualified requesters may obtain copies of this report from DDC, Cameron Station, Alexandria, Va. Orders will be expedited if placed through the librarian or other staff member designated to request and receive documents from DDC.

When Government drawings, specifications or other data are used for any purpose other than in connection with a definitely related Government procurement operation, the United States Government thereby incurs no responsibility nor any obligation whatsoever; and the fact that the Government may have formulated, furnished, or in any way supplied the said drawings, specifications, or other data, is not to be regarded by implication or otherwise as in any manner licensing the holder or any other person or corporation, or conveying any rights or permission to manufacture, use, or sell any patented invention that may in any way be related thereto.

GASDYNAMIC DIAGNOSIS OF HIGH-SPEED FLOWS  
EXPANDED FROM PLASMA STATES

By

J. Leith Potter, George D. Arney, Jr.

Max Kinslow, and William H. Carden

von Kármán Gas Dynamics Facility

ARO, Inc.

a subsidiary of Sverdrup and Parcel, Inc.

November 1963

ARO Project No. VL2407

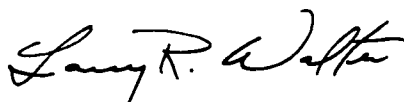
**ABSTRACT**

The report describes a number of methods of determining quantities which define the flow in low-density, hypersonic wind tunnels which use plasma generators to heat the working fluid. Although the fluid was heated to a plasma state initially, with a typical bulk temperature of 12,000°R, the measurements reported were for the purpose of calibrating the flow in the aerodynamic nozzle of a wind tunnel where it is desirable that the fluid be recombined before or during the expansion to high speeds.

All of the methods considered may be classed as gasdynamic or aerodynamic as opposed to, say, spectroscopic methods. Measurements of total enthalpy, total and static pressure, and local mass flux are discussed, with descriptions of the equipment and typical results included. The emphasis is placed on procedures not requiring assumptions for the data reduction which cannot be checked. An appendix containing an account of the effect on nozzle flow which was caused by one method of swirling gas injection into the plasma generator electrode section is also included.

**PUBLICATION REVIEW**

This report has been reviewed and publication is approved.



Larry R. Walter  
1st Lt, USAF  
Gas Dynamics Division  
DCS/Research

  
Donald R. Eastman, Jr.  
DCS/Research

## CONTENTS

	<u>Page</u>
ABSTRACT . . . . .	iii
NOMENCLATURE . . . . .	vii
1.0 INTRODUCTION . . . . .	1
2.0 THE WIND TUNNEL . . . . .	1
3.0 DIAGNOSTIC METHODS	
3.1 The Total Calorimeter . . . . .	3
3.1.1 The Calculation of Total Enthalpy . . .	3
3.1.2 Experimental Data . . . . .	5
3.2 Impact-Pressure Probe . . . . .	7
3.3 Static-Pressure Probe . . . . .	8
3.4 Local Total-Enthalpy Probe . . . . .	10
3.5 Mass-Flux Probe . . . . .	12
4.0 CONCLUDING REMARKS . . . . .	14
REFERENCES. . . . .	14
APPENDIX I: Plasma Swirl . . . . .	33

## TABLE

1. Tunnel L Operating Conditions with Arc Heater . . . . .	16
--	----

## ILLUSTRATIONS

### Figure

1. Photograph of Gas Dynamic Wind Tunnel, Hypersonic (L) from the Operator's Side . . . . .	17
2. Schematic Sketch of Arc-Heated Wind Tunnel . . . . .	18
3. Total Calorimeter . . . . .	19
4. Stagnation Enthalpy as a Function of $\dot{m}$ , $p_o$ , and $A^*$ . .	20
5. Total Calorimeter Results for 2-in. Stilling Chamber . . . . .	21
6. Total Calorimeter Results for 3-in. Stilling Chamber . . . . .	22
7. Total Calorimeter Results for 5-in. Stilling Chamber . . . . .	23

<u>Figure</u>	<u>Page</u>
8. Total Calorimeter Results for 8-in. Stilling Chamber . . . . .	24
9. Variation of Measured Impact Pressure with Orifice-to-Probe Diameter Ratio (Argon Gas, Reservoir Temperature = 7660°R, $M_\infty = 8.2$ , $T_w/T_o \approx 0.19$ ). . . . .	25
10. Static-Pressure Probe . . . . .	26
11. Local Total-Enthalpy Probe. . . . .	27
12. Photograph of Local Total-Enthalpy Probe in Hypersonic Argon Flow. . . . .	28
13. Results from Local Total-Enthalpy Probe in the Low-Density, Arc-Heated Tunnel . . . . .	29
14. Schematic Diagram of Mass-Flux Probe System . . . . .	30
15. Comparison of Measured and Calculated Local Mass Flux, $\rho_\infty U_\infty$ . . . . .	31
16. Effect of Increased Time Interval on Measured Mass-Flux . . . . .	32

## NOMENCLATURE

A	Cross-sectional area
a	Speed of sound
$C_p$	Specific heat at constant pressure
d	Diameter
f	Friction coefficient
f	"Function of"
H	Enthalpy
Kn	Knudsen number
L	Axial length of settling chamber
M	Mach number
m	Mass
$\dot{m}$	Mass-flow rate
Pr	Prandtl number
p	Pressure
$p_o'$	Total pressure downstream of a Rankine-Hugoniot (R-H) type of normal shock wave
Q	Heat-transfer rate
$\dot{q}$	Heat-transfer rate per unit area
R	Radius of outer shell of impact-pressure probe
R-H	Rankine-Hugoniot type normal shock wave
r	Radius of orifice in impact-pressure probe
S	Entropy
T	Temperature
t	Time
U	Velocity in axial direction downstream in nozzle
V	Volume of tank of mass-flux probe system
x	Axial coordinate
$\gamma$	Ratio of specific heats of gas medium
$\epsilon$	$\rho_\infty/\rho_2$ , based on R-H normal shock wave
$\lambda$	Mean free path in gas medium



$\mu$	Normal coefficient of viscosity
$\rho$	Mass density of gas medium

#### SUBSCRIPTS

2	Evaluated immediately downstream of a R-H normal shock wave
aw	Adiabatic recovery temperature or enthalpy
cold	Condition at transducer, assumed to be at cooler end of tube
i	Indicated impact pressure
o	Total or reservoir value
p	Indicates probe value
w	Wall temperature
$\infty$	Free-stream value

#### SUPERSCRIPT

*	Evaluated at sonic throat of nozzle
---	-------------------------------------

## 1.0 INTRODUCTION

Considerable experience has been gained at the Arnold Engineering Development Center\* relative to the use of plasmas as sources of high-enthalpy fluid for gasdynamics applications. The particular experience of the authors is derived from their use of plasmas in connection with a low-density, hypersonic, continuous-type wind tunnel. Calibration of this facility has involved more attention to flow diagnosis than is ordinarily the case with other high-speed wind tunnels. It is the purpose of this report to describe certain techniques used and results obtained in the course of this work. Only gasdynamic (or aerodynamic) techniques are discussed.

## 2.0 THE WIND TUNNEL

A detailed description of the wind tunnel is not necessary because it is intended to concentrate attention on techniques of diagnosis not necessarily restricted to a specified facility. However, a brief description has some value inasmuch as it defines physical dimensions and characteristics of the fluid flow.

The tunnel that was used is a continuous-type, arc-heated, ejector-pumped design. The major components are, in streamwise order,

1. D-C arc-heater (Thermal Dynamics U-50), with 40-kw power supply;
2. Settling section of variable size but normally of 3-in. diam and 6.25- to 10-in. length;
3. Aerodynamic nozzle of variable size with 0.10- to 0.75-in. -diam throat and 2.0- to 6.0-in. -diam exit;
4. A tank of 48-in. diam surrounding the test section and containing instrumentation and probe carrier;
5. Interchangeable diffuser;
6. Water-cooled heat exchanger;
7. Air-ejector of two stages; and
8. The VKF mechanical vacuum-pumping system.

---

\*The work reported herein was done in the Research Branch, von Kármán Gas Dynamics Facility (VKF), Arnold Engineering Development Center (AEDC), Air Force Systems Command (AFSC).

Manuscript received October 1963.

All critical components of the tunnel are protected by back-side water cooling. The two-stage ejector system is driven by air instead of steam because of the ready availability of high-pressure air at the tunnel site. The working gas normally is nitrogen or argon, although other gases may be used. Typical ranges of operation with heated flow are given in Table 1, and Fig. 1 is a photograph of the tunnel.

Figure 2 is helpful in understanding the type of flow process studied. A plasma generator is used because it provides the means to heat a variety of gases to the enthalpy levels required for obtaining hypervelocity flow. In fact, it expels the gas in a condition considered undesirable for most of the studies conducted with the wind tunnel before this time, i. e., the aerodynamics of low-density flows. Therefore, the plasma is allowed to flow across a relatively large settling chamber before being admitted to the aerodynamic nozzle. Acceptable degrees of thermo-chemical equilibrium, flow steadiness, and uniformity of gas properties must be achieved in the settling section. A significant heat loss is also incurred, and one is motivated to study the effect of settling section geometry on heat loss as well as the character of flow leaving this section. However, only the latter is of concern in this report.

Downstream of the settling section the fluid enters a contraction section, the nozzle throat, and the expansion section of the nozzle in that order. The test section is located at the end of the hypersonic nozzle. If flow properties in the test section are to be determined by methods which refer to total pressures or enthalpies measured in the settling section, it is necessary to ensure the existence of an inviscid or, more precisely, an influscid\* core of flow throughout the nozzle. This alone is not enough; the thermo-chemical state of the gas throughout the expansion from its plasma state must also be established because of the danger that nonequilibrium processes of de-excitation and recombination may invalidate the theory by which flow properties in the test section are derived. For example, this can occur when the ratio of impact pressure at the test section to total pressure in the settling section is used in combination with, say, the equilibrium gas equations to calculate flow properties.

The subsequent sections will deal with various techniques that have been used by the authors and their colleagues for diagnosing the flow in the small tunnel described here. This is not intended to be an exhaustive account of all useful methods available. A moderate degree of familiarity with the subject is assumed.

---

\*A term believed to have been originated by Dr. Sinclair M. Scala and intended to indicate, in the present case, the absence of lateral flux from the core flow by any processes such as diffusion, conduction, viscosity, etc.

### 3.0 DIAGNOSTIC METHODS

The need to apply a number of independent procedures for flow diagnosis is apparent. Unfortunately, several of the measurements that may be made accurately and interpreted easily when dealing with conventional tunnels are not useful when low densities and high speeds are combined. It should not be assumed that the techniques included herein are completely free of restrictions. The important point made here is the obvious one that no single measurement should be relied on without independent confirmation by other means, if that is possible.

#### 3.1 THE TOTAL CALORIMETER

One of the basic flow characteristics is total enthalpy. Many investigators have determined this by subtracting cooling losses from electrical energy input to the electrodes and assuming that the remainder was total enthalpy of the fluid. This is a valid procedure if the required degree of measurement accuracy is achieved. Several years ago it was not unusual to find investigators relying on spectroscopic methods of temperature measurement. Often they quoted extremely high enthalpies. It developed that many of these results were erroneous because the gas was not in equilibrium and the electron temperature did not truly represent the fluid (cf Ref. 1).

Both of the procedures mentioned are usually inferior in experimental accuracy to a direct measurement of stream total enthalpy by using a calorimeter as shown in Fig. 3. The method described here also yields clues concerning both thermo-chemical state of the gas and flow uniformity at the throat of the aerodynamic nozzle because it is possible to apply theoretical methods to the calculation of total enthalpy on the basis of measured mass-flow rate, total pressure, and nozzle geometry in the throat region. Comparison of measured and theoretical results can lead to a fuller understanding of the flow process. The theoretical analysis will be outlined first.

##### 3.1.1 The Calculation of Total Enthalpy

The total enthalpy may be calculated on the basis of quantities that are readily measured. If the mass-flow rate through the nozzle, the total pressure, and the nozzle area at the sonic point are known and if the gas is in equilibrium from the settling chamber to the sonic point, or if another known thermo-chemical condition exists, the enthalpy is uniquely determined. The mass-flow rate, nozzle dimensions, and the total pressure may be measured directly, but the thermo-chemical state of the gas

often is questionable. In this section, the latter question is ignored and attention is concentrated on the calculation procedure for an assumed thermo-chemical flow model.

To obtain an estimate of the effective area of the nozzle at the sonic point, one-dimensional flow\* in thermodynamic equilibrium was assumed for the case of concern to the present authors. The equations for this type of flow can be found from a table of influence coefficients following Shapiro and Hawthorn (Ref. 2). The influences of area change, heat transfer, and wall friction on Mach number are given by the following equations:

$$\frac{dM^2}{M^2} = \frac{1}{1-M^2} \left[ -2 \left( 1 + \frac{\gamma-1}{2} M^2 \right) \frac{dA}{A} + \left( 1 + \gamma M^2 \right) \frac{dQ}{\dot{m} C_p T} + 4\gamma M^2 \left( 1 + \frac{\gamma-1}{2} M^2 \right) \frac{f dx}{d} \right] - \frac{d\gamma}{\gamma} \quad (1)$$

At the sonic point,  $M = 1$ , and the quantities  $dM^2/M^2$  and  $d\gamma/\gamma$  remain finite. This requires that

$$(dA/A)_{M=1} = dQ/(\dot{m} C_p T^*) + (2\gamma f/d) dx \quad (2)$$

From Eq. (2) it is seen that, in the absence of heat transfer, skin friction would result in a positive  $dA/A$  at the sonic point. This can occur only in the diverging section of the nozzle. Similarly, in the absence of skin friction, heat removal from the fluid will necessitate the sonic point being in the converging section.

To more adequately determine the location of the sonic point in a particular case of concern to the authors, an estimate of the heat loss and skin friction was made for a typical set of operating conditions ( $T_0 = 5400^\circ R$ ,  $p_0 = 17.79$  psia, and  $\dot{m} = 3.616$  lb<sub>m</sub>/hr). The boundary-layer calculation method of Cohen and Reshotko (Ref. 3) was used. Upon substitution of estimated values into Eq. (2), it was found that the sonic point was approximately 0.012 in. upstream of the geometric throat for this particular set of conditions. This implies an  $A^*$  which is only 0.28 percent greater than the geometric throat area. As a different approach, the boundary-layer displacement thickness at the throat also was calculated by the method of Ref. 3 and found to increase the effective  $A^*$  by 0.66 percent. In view of the result and the probable accuracy of these calculations, it is assumed that the nozzle cross-sectional area

---

\*Note that this assumption disregards the more likely flow model consisting of an influscid core surrounded by a boundary layer.

at the sonic point is equal to the minimum geometric area in the normal operation of the low-density tunnel.

If it is assumed that the flow in the nozzle is isentropic and adiabatic and, furthermore, that the flow is in equilibrium, the following relationship may be written:

$$S_o = S^* \quad (3)$$

and

$$H_o = H^* + \frac{1}{2} (a^*)^2 \quad (4)$$

After assuming the enthalpy and the entropy of the gas at the sonic point, the speed and density at that point can be determined from a table of the thermodynamic properties of the working gas. Thus, Eqs. (3) and (4) yield the total enthalpy and entropy from which total pressure can be determined for a set of assumed conditions.

Using the equation of mass conservation,

$$\dot{m} = \rho^* a^* A^* \quad (5)$$

it is easily shown that

$$\dot{m}/(p_o A^*) = \rho^* a^*/p_o = f(H_o, p_o) \quad (6)$$

Since  $\rho^*$ ,  $a^*$ ,  $p_o$ , and  $H_o$  may be related, the function  $f(H_o, p_o)$  is determined at  $H_o$ . Additional sonic point conditions may be chosen until  $f(H_o, p_o)$  is completely determined, and a graphical relation such as shown in Fig. 4 may be prepared for an assumed thermo-chemical flow model. This may be used thereafter as a working figure from which  $H_o$  may be read after  $\dot{m}/(p_o A^*)$  is measured.

### 3.1.2 Experimental Data

The total calorimeter shown in Fig. 3 was designed to duplicate, for all practical purposes, the configuration of the tunnel upstream of the geometric throat of the nozzle. Downstream of the throat, in place of the nozzle, the calorimeter contains a heat exchanger to extract energy from the gas stream.

The upstream portion of the calorimeter consists basically of the interchangeable, cylindrical settling section and the converging, aerodynamic nozzle section. These two sections, as well as the downstream heat exchanger, are independently water-cooled, and provisions are made for measuring water-flow rates and temperature differences between incoming and exhaust water flows. The upstream end of the settling section

is flanged to receive the plasma generator. The cooled gas is exhausted from the calorimeter to the vacuum pumping system. The gas temperature is measured at the heat exchanger exit in order to find the remaining or residual enthalpy.

A calorimetric study was conducted (Ref. 4) to establish the settling-chamber length required to justify the assumption of uniformity and equilibrium in the reservoir and to provide an experimental check on the method discussed in Section 3.1.1 for determination of total enthalpy on the basis of measured pressure, flow rate, minimum nozzle throat area, and assumed equilibrium and uniform flow. The results of these experiments are shown in Figs. 5 through 8, where the total enthalpy is plotted as a function of  $\dot{m}/p_0$  for various settling chamber lengths. Also shown by the solid-line curve is the theoretical value of enthalpy that should exist for a given  $\dot{m}/p_0$  if uniform, equilibrium, sonic flow exists at the nozzle minimum area. It should be noted that the experimentally determined total enthalpy is greater than the theoretical value for the 2-in. length but appears to approach the theoretical value as a limit when the length is increased. For the 5- and 8-in. lengths, the agreement of measurement and theory is good.

Consideration of the flow pattern in the settling chamber reveals that such a trend might well be expected. Visualize a highly energetic, nonequilibrium, nonuniform gas exiting the arc heater in a concentrated jet with an average temperature approximately 13,000°R in the examples referred to here. Unless sufficient mixing length is provided for this high-speed flow to diffuse and nearly come to rest before entering the aerodynamic nozzle, it may be expected that such flow will enter the throat in a nonuniform state. Moreover, unless the settling chamber is sufficiently long, and/or sufficiently high densities exist, nonequilibrium of the working gas may persist to the vicinity of the aerodynamic throat. Only a small mass fraction of the gas need be dissociated or ionized to represent a significant amount of energy. Either possibility could lead to results such as those shown when  $L < 5$  in. in the present experiments. Furthermore, if the minimum-area section of the nozzle is appreciably different from the sonic area, as it will be if diabatic-flow and boundary-layer influences are great enough, then the computed total enthalpy will be in error.

Generally speaking, several factors could be expected to influence the degree to which uniformity and equilibrium are achieved before entrance of the working gas into the aerodynamic throat. Aside from the operating condition itself, the geometry of the arc-heater anode orifice, the area contraction between settling section and aerodynamic throat, the amount of swirl (if any) given the gas in the arc heater, and the length and diameter of the settling chamber might be among the

governing factors. However, for the geometry and range of operating conditions considered in the present case where there is no swirl and the plasma jet diameter is approximately 0.26 in., it is apparent that a settling chamber length of 5 in.  $< L < 8$  in. with a diameter of 3 in. is sufficient to cause measured total enthalpy to closely match the calculated, ideal case. This indicates that the several factors expected to introduce errors in the computed value of total enthalpy are either negligible or are compensating for each other. Since it is difficult to believe that such perfect compensation would result over the entire range of conditions for which data were obtained, it is implied that the flow at and immediately upstream of the throat does not deviate far from the idealized flow model; i. e., for all practical purposes, the flow is uniform and in thermo-chemical equilibrium under the particular conditions studied when  $L > 5$  in. However, it is obvious that these results may not apply in a quantitative sense when different conditions exist, and the question must be re-examined by each investigator. The influence of one type of swirling fluid injection in the electrode region is discussed in Appendix I.

### 3.2 IMPACT-PRESSURE PROBE

This is the device most widely used for a study of flows in wind tunnel nozzles. Since a recent paper by one of the present authors and a colleague (Ref. 5) reports a study of such probes, an extensive discussion is not included herein.

It will only be remarked that a flat-nosed impact-pressure or pitot probe appears to be free of Reynolds number influence, i. e.,  $p_i = p_0^*$  when

$$(\rho_\infty U_\infty R / \mu_2) (\rho_2 / \rho_\infty)^{1/2} > 1000 \quad (7)$$

If approximately 5 percent error is acceptable, the above limit may be reduced considerably (cf Ref. 5). However, no general rule may be given in simple form, and the investigator must study his own particular case. The given limit is drawn from Ref. 5 and is based on experiments in essentially perfect gases where  $1.8 \leq M_\infty \leq 10.7$ ,  $\gamma = 1.400$  or  $1.667$ , and  $0.1 \leq T_w / T_{aw} \leq 1.0$ .

When Reynolds numbers are very low, it has been shown in Ref. 6 that the orifice diameter may become a factor as illustrated in Fig. 9. The basic reason for this is not entirely clear, although it has been suggested that the thermal transpiration phenomenon may be a factor. On the other hand, it is interesting to note that, in the data available to



the authors, the impact pressure shows an effect of orifice size regardless of probe Reynolds number based on outside radius when

$$(\rho_{\infty} U_{\infty} r / \mu_s) (\rho_s / \rho_{\infty})^{1/2} \gtrsim 5 \quad (8)$$

However, bearing in mind the possibility that the temperature field in the neighborhood of the orifice may be important, the relation just written may not be completely general. When condition (7) exists, it is unnecessary that condition (8) exist.

A problem arises if relatively large impact-pressure probes are used in flows wherein there are large gradients in impact pressure, e.g., when surveying a small, freely expanding jet or flow in a small, conical nozzle. Note that the pressure read from a probe being used in a flow with an axial gradient in impact pressure corresponds to a point upstream of the orifice a distance equal to shock wave stand-off distance (cf Ref. 5).

It is clear that the impact-pressure probe is not completely free of all sources of error. However, attention to such matters as those just referred to can permit its use to good effect in calibrating flows.

### 3.3 STATIC-PRESSURE PROBE

Probes of the type shown in Fig. 10 are seldom used in hypersonic gas streams because such applications usually involve strong pressure interaction effects. This source of error arises because the boundary layer effectively changes the shape of the probe and generally causes the measured pressure to be higher than the free-stream static pressure, cf Ref. 7. Pressure interaction analyses have appeared in the gasdynamics literature. Although the type of probe sketched in Fig. 10 is not an "aerodynamic" flat plate, the finite thickness is not particularly important in the present context. Thus, it may be considered essentially the same as a flat plate. From Ref. 8, p. 345, one finds, for flat-plate flow and for the weak interaction regime which should characterize a static-pressure probe,

$$p/p_{\infty} = 1 + \gamma D_o \bar{\chi}_o + \gamma(\gamma + 1) D_o^2 \bar{\chi}_o^2 / 4 + \dots \quad (9)$$

where  $D_o = A T_w / (M_{\infty}^2 T_{\infty}) + (\gamma - 1) B$  (See table on following page.)

$$\bar{\chi}_o = M_{\infty}^3 (C_{\infty} / Re_{x_{\infty}})^{1/2}$$

$$C_{\infty} = (\mu_w / \mu_{\infty}) (T_{\infty} / T_w)$$

$$Re_{x_{\infty}} = \rho_{\infty} U_{\infty} x / \mu_{\infty}$$

Pr =	1.00	0.725
A =	0.865	0.968
B =	0.166	0.145

Equation (9) does not account for vorticity, transverse curvature, slip, variable surface temperature, or influence of the induced pressure gradient on boundary-layer growth rate. However, Eq. (9) is adequate to show that if errors in measured free-stream static pressure are to be kept to the order of, say, two percent, it is necessary that  $Re_{x_\infty} \gg M_\infty^6$ . For example, let  $M_\infty^2 \gg 1$ ,  $\gamma = 1.40$ ,  $Pr = 0.725$ , and  $T_w = T_\infty$ . Then it follows that

$$p/p_\infty \approx 1 + \gamma(\gamma-1) B M_\infty^3 / (Re_{x_\infty})^{1/2} + \dots \quad (10)$$

Or, if 2 percent error is allowable, it is necessary that

$$Re_{x_\infty} > 16 M_\infty^6 \quad (11)$$

When the same conditions exist, except with  $\gamma = 1.67$ , the requirement is

$$Re_{x_\infty} > 64 M_\infty^6 \quad (12)$$

At very low Reynolds numbers, slip would decrease the pressure interaction effect, but this obviously does not change the conclusion implied by the foregoing considerations.

Another important possible cause of error when measuring low pressures in heated flows is the thermal transpiration effect, cf Refs. 7 and 9. To illustrate, let it be assumed that wall surface temperature at the point where pressure is to be measured is 1040°R while transducer temperature is 520°R. Let the inside diameter of the tube connecting orifice and transducer be 0.1 in., and let the pressure at the transducer be read as 0.001 psia, or 51.7 microns Hg. One finds, for argon, air, or nitrogen, that Knudsen number at the transducer (cold) end of the connecting tube is approximately 0.8, based on tube radius. Following Ref. 9, this yields the result that pressure as read by the transducer is 82 percent of the true pressure at the orifice where pressure is to be determined. For negligible error that is caused by thermal transpiration, under the conditions stipulated above, tube diameter would have to be increased about thirty times (3-in. diam) or wall temperature decreased to near transducer temperature. When transducers are near normal room temperature, avoidance of thermal transpiration influence generally requires

$$Kn_{cold} = (\lambda_{cold} / \text{tube radius}) < 0.01 \quad (13)$$

for practical cases. Thus, use of free-stream static pressure measurements that are made when low-density, hypersonic, high-enthalpy

conditions exist is questionable. With exercise of sufficient care, useful data may be obtained, but primary calibration must rest on other measurements.

### 3.4 LOCAL TOTAL-ENTHALPY PROBE

One of the more useful measurements in the test section is the local total enthalpy. In view of the widely demonstrated, approximate agreement between theory and experiment for heat-transfer rate to a stagnation region of a simple body, many have used a measured heat-transfer rate substituted into the Fay-Riddell or other appropriate equation to determine local total enthalpy indirectly. This procedure is not unreasonable because heat-transfer rate in hypersonic flow is dominated by the difference between local total and wall enthalpies. However, aside from concern for measurement accuracy, certain other precautions must be taken.

For example, a problem arises if the degrees of gas dissociation and ionization and the catalytic properties of the probe surface are unknown. Also, current experimental data from tests with stream velocities greater than 20,000 fps scatter by  $\pm 30$  percent. Therefore, it is far better to use the indirect method, which relies on an assumed theoretical flow model, only when there is adequate assurance that the flow model applies. For less well understood cases, a direct measurement is preferable.

The probe shown in Fig. 11 has been used by the authors. The probe is axisymmetric and consists essentially of a water-cooled inner jacket and a water-cooled outer jacket with thermal insulation sandwiched in between. Each jacket is knife-edged at the front with a clearance of 0.002 to 0.005 in. to reduce heat transfer between jackets. Now, if the bow shock is swallowed, it can be assumed that the total energy per unit time entering the inner jacket is the product of the total enthalpy, probe entrance area, local free-stream density, and velocity ( $H_0 A \rho_\infty U_\infty$ ). This product also can be obtained from calculations based on an assumed flow model, and the results of such calculations may be compared with the measurements.

Similarly for the total calorimeter, the assumption is made that the total energy entering the probe can be accounted for by measuring the water flow rate and temperature rise and the total temperature of the exiting gas. There are several points at which failure may occur when accurate data are desired from this probe. First, there is the chance that the bow shock may not be completely swallowed. Also, there is the possibility of heat transfer between the inner and outer shell

which can, of course, be minimized by controlling the water flow rates so that a minimum temperature difference is maintained between them. The internal heat transfer is likely to vary with mass-flow rate through the probe as well as  $H_0$  and the flow field at the inlet; thus determination of probe "tare" data is not readily accomplished by simply shutting off the internal flow and considering the resulting probe indication to be the correct tare value. Thirdly, it may be possible for energy to be frozen in certain modes that will not be detected by the probe. Finally, the probe must be relatively large, and there is the chance of distorting the nozzle flow approaching the probe. The last may occur because of blockage or the upstream influence of the flow field of the probe.

With the probe located at a known position in the tunnel test section and in the core of uniform flow, a set of standard tunnel operating conditions was established, and the cooling water to the probe was adjusted so that the inlet and outlet water temperatures at the outer jacket were approximately equal to the corresponding ones at the inner jacket. After the probe had reached an equilibrium temperature throughout, the necessary measurements were made and recorded. A photograph of the probe in use is shown in Fig. 12.

A typical set of results taken in argon flow in the manner described above is shown in Fig. 13, where the measured quantity,  $H_0 A \rho_\infty U_\infty$ , is compared to the theoretical value obtained from impact pressures with assumed isentropic flow from reservoir conditions established by the method given in Section 3.1.1. The case represented in Fig. 13 obviously is one wherein the assumed flow model was correct, i. e., negligible chemical kinetic effects and incompressible nozzle core flow. Agreement does not always result, and it is in such cases that the local total calorimeter probe is most valuable.

Although it has been found that the bow shock is readily swallowed in hypersonic flows, even at low densities, it probably is better to design the total-enthalpy probe so that mass flux also is measured. If  $(A \rho U)$  is measured directly, as well as  $(H_0 A \rho U)$ , it is not essential that the total-enthalpy probe swallow its bow shock wave, and the probe can be made more compact.

To conclude, the authors feel that the total-enthalpy probe is a very useful device when used in connection with other methods of measurement. It is often an imperfect calorimeter, and this should be kept in mind.

### 3.5 MASS-FLUX PROBE

Preliminary results, originally reported in Ref. 10, have encouraged the authors to investigate further the suitability of a mass-flux probe as a calibrating device in high-enthalpy, hypersonic flow. The object of this probe is to obtain a measure of the local product  $(\rho_\infty U_\infty)$  in the expanded flow. Obviously, if this product can be measured, the result can be compared to the value computed on the basis of impact-pressure measurements referred to reservoir- or total-pressure measurements, and agreement would constitute added proof of the accuracy of all other calibration data based on a given model of the nozzle core flow. Moreover, in hypersonic flow, impact pressure

$$p_o' \approx \rho_\infty U_\infty^2 (1 + \epsilon/2) \quad (14)$$

Thus, one may obtain reasonably accurate values of  $\rho_\infty$  and  $U_\infty$  directly from combining impact- and mass-flow probe measurements in hypersonic flow because  $\epsilon \ll 1$  and is insensitive to variations in  $M$  when  $M$  is large.

The apparatus used in this extension of the original work is shown schematically in Fig. 14. A typical data point is obtained by allowing the fluid to flow into the probe and then enter an evacuated vessel of known volume,  $V$ , for a measured time interval,  $\Delta t$ . The masses of gas in the vessel at the beginning and end of the time interval are determined from ordinary pressure and temperature measurements. The mass-flow rate is then given by

$$\dot{m} = (m_t - m_1) / \Delta t \quad (15)$$

where  $(m_t - m_1) = \Delta m$ , the mass captured in the interval  $\Delta t$ . Now, if the bow shock is swallowed throughout the time interval,

$$\dot{m} = \rho_\infty U_\infty A_p \quad (16)$$

and, by combination of Eqs. (15) and (16),

$$\rho_\infty U_\infty = (m_t - m_1) / (A_p \Delta t) \quad (17)$$

Also, at each data point the impact pressure was measured by use of the mass-flux probe itself. This was done by blocking the flow in the tube leading from the probe and measuring the pressure therein. (Barring mechanical complications, one obviously may measure  $H_o A \rho_\infty U_\infty$ ,  $A \rho_\infty U_\infty$ , and  $p_i$  with a single probe.)

Unfortunately, because of the small size of the probe and normal limitations in machining the 0.1-in. -diam probe tip, it was not possible to determine the "aerodynamic" inlet area by mechanical measurements to the desired accuracy. With a microscope it was found that the knife-edged inlet was relatively dull and also that the inlet was not perfectly

circular. The area actually used throughout the data analysis was determined by taking calibration data in unheated flow of  $M_\infty = 6.9$ . In this case, flow properties determined from impact pressure and assumed isentropic flow at relatively high Reynolds number should be accurate. A larger probe of 0.25-in. -diam inlet was tested under the same circumstances and found to have a calibration factor of 1.02. Thus, the calibration of the small probe seems validated by the result from the larger probe where uncertainty regarding the inlet area was a minor point.

In Fig. 15 the measured  $(\rho_\infty U_\infty)$  is compared to the theoretical  $(\rho_\infty U_\infty)$ . The latter was obtained from the ratio of impact pressure to total pressure and the method of Section 3.1.1 for total enthalpy, with frozen flow assumed throughout for all of the different flow conditions. These conditions were such that Reynolds number was large enough that no significant errors should have existed in measuring  $p_0^*$ . Data from both 0.1- and 0.25-in. -diam probes are included in Fig. 15.

A most important requirement in the mass-flux measurements is that the bow shock at the probe inlet be swallowed. If this is not the case, the effective inlet area will not be constant for varying conditions and cannot be defined. In the present tests, two observations were made which indicate that the shock was swallowed. First, mass-flux measurements were made for extended time intervals which allowed the pressure in volume V to attain higher values than ordinarily used. If the shock were not swallowed, it was expected that the increased pressure would alter the mass-flow rate into the tank. The results shown in Fig. 16 reveal that the mass flux was constant for  $\Delta t < 1000$  seconds in that case.

Secondly, the probe was tested in supersonic flows where there was sufficient glow from radiating species to observe the bow shock. With flow through the probe blocked, the shock was observed to stand off in front of the probe entrance. Immediately upon applying the normal suction to the probe, the shock appeared to be swallowed.

A degree of uncertainty exists in regard to possible rarefied-flow influences on the mass-flux probe. The present authors have a small amount of data from experiments at very low Reynolds numbers, and these data indicate that the measured mass flux is in error when

$$(\rho_\infty U_\infty r/\mu_s) < 5 \quad (18)$$

This must be regarded as a tentative limitation at present, particularly inasmuch as it is far from obvious that the parameter in the above

inequality is the appropriate one. These remarks are included in order to warn potential users of this type of probe that caution is indicated when very low Reynolds numbers are concerned. Above the given limit, results such as those in Fig. 15 have been obtained.

#### 4.0 CONCLUDING REMARKS

The methods described herein have proved to be useful for flow diagnosis. The design of the probe systems and application of the methods are relatively simple. Even the more elaborate probes have been in use for several years at least, and, of course, the pressure probes are as old as the study of fluid mechanics. In Ref. 11, a probe combining measurements of total enthalpy, mass flux, and impact pressure was proposed, but no data were given. In Ref. 12, a probe for local total enthalpy was described, and some data were reported. The present authors and their colleagues have been using total-enthalpy and mass-flux probes of the type discussed for about three years and have found them to be essential aids when used carefully and in combinations allowing a degree of independence in compared results. When these gasdynamic methods are supplemented by the various electrical, electronic, and spectrographic techniques, a thorough diagnosis of flows expanded from plasma states usually is possible.

#### REFERENCES

1. Dooley, M. T., McGregor, W. R., and Brewer, L. E. "Characteristics of the Arc in a Gerdien-Type Plasma Generator." ARS Journal, Vol. 32, No. 9, Sept. 1962, pp. 1392 - 1394.
2. Crocco, L. "One-Dimensional Treatment of Steady Gas Dynamics." Sect. B. of Fundamentals of Gas Dynamics, Ed. by H. W. Emmons, Princeton University Press, Princeton, N. J., 1958, pp. 256 - 263.
3. Cohen, Clarence B. and Reshotko, Eli. "The Compressible Laminar Boundary Layer with Heat Transfer and Arbitrary Pressure Gradients." NACA TR-1294, 1956.
4. Arney, George D., Jr. and Boylan, David E. "A Calorimetric Investigation of Some Problems Associated with a Low-Density Hypervelocity Wind Tunnel." AEDC-TDR-63-19, Feb. 1963.

5. Potter, J. Leith and Bailey, Allan B. "Pressures in the Stagnation Regions of Blunt Bodies in the Viscous-Layer to Merged-Layer Regimes of Rarefied Flow." AEDC-TDR-63-168, September 1963.
6. Bailey, Allan B. and Boylan, David E. "Some Experiments on Impact-Pressure Probes in a Low-Density, Hypervelocity Flow." Proc. of the 1962 Heat Transfer and Fluid Mech. Inst., Ed. by F. E. Ehlers, et al., Stanford Univ. Press, 1962, pp. 62-75.
7. Boylan, David E. "An Analysis of Initial Static Pressure Probe Measurements in a Low-Density, Hypervelocity Wind Tunnel." AEDC-TDR-63-94, April 1963.
8. Hayes, W. D. and Probstein, R. F. Hypersonic Flow Theory. Academic Press, 1959, p. 345.
9. Arney, George D., Jr. and Bailey, Allan B. "The Effect of Temperature on Pressure Measurements." To be published in AIAA Journal.
10. Potter, J. L., Kinslow, M., Arney, G. D., Jr., and Bailey, A. B. "Initial Results from a Low-Density Hypervelocity Wind Tunnel." Hypersonic Flow Research, Ed. by F. R. Riddell, Academic Press, 1962, pp. 599 - 624.
11. Christensen, Daphne and Buhler, Rolf D. "Arc Jet Tunnel Development and Calibration for Parabolic Re-entry Simulation." Plasmadyne Corp. Rept. 1FR011-1872, 3 June 1961.
12. Grey, J., Jacobs, P. F., and Sherman, M. P. "Calorimetric Probe for Measurement of Extremely High Temperatures". Review of Scientific Instruments. Vol. 33, No. 7, July 1962, pp. 738 - 741.



TABLE 1  
TUNNEL L OPERATING CONDITIONS WITH ARC-HEATER

	<u>Nitrogen</u>	<u>Argon</u>
Total pressure, psia	7.0-29.4	0.5-6.4
Total enthalpy, Btu/lb <sub>m</sub>	740-2130	280-960
Total temperature, °R	2300-7200	2300-7700
Mach number	4.8-10.8	3.7-16.1
Unit Reynolds number, free stream, in. <sup>-1</sup>	300-3500	270-4700
Unit Reynolds number behind normal shock, in. <sup>-1</sup>	35-1140	14-1080
Mean free path, free stream, billiard-ball gas model, in.	0.002-0.058	0.002-0.057
Uniform flow core diameter at test section, in.	0.2-1.2	0.5-1.5

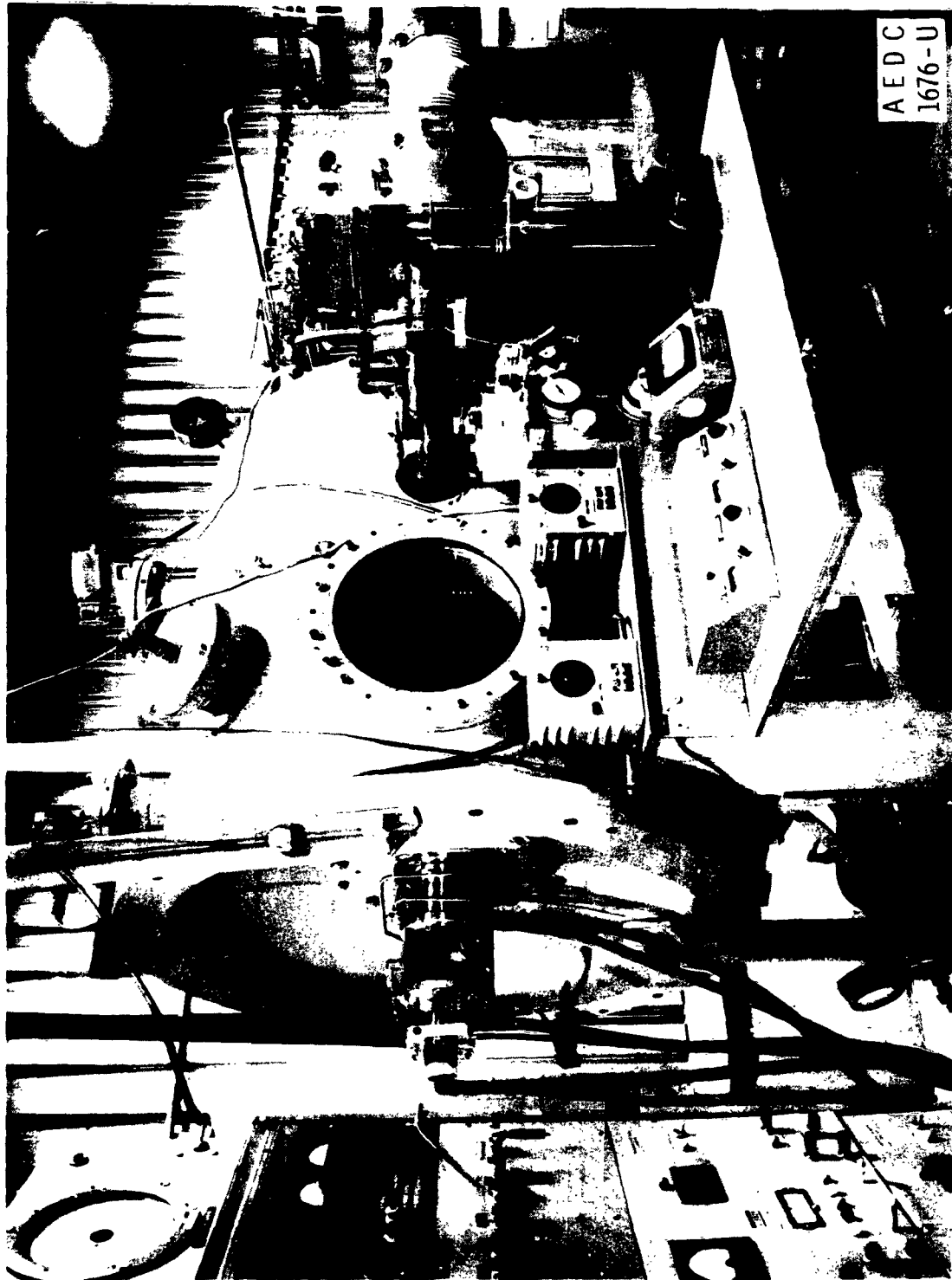
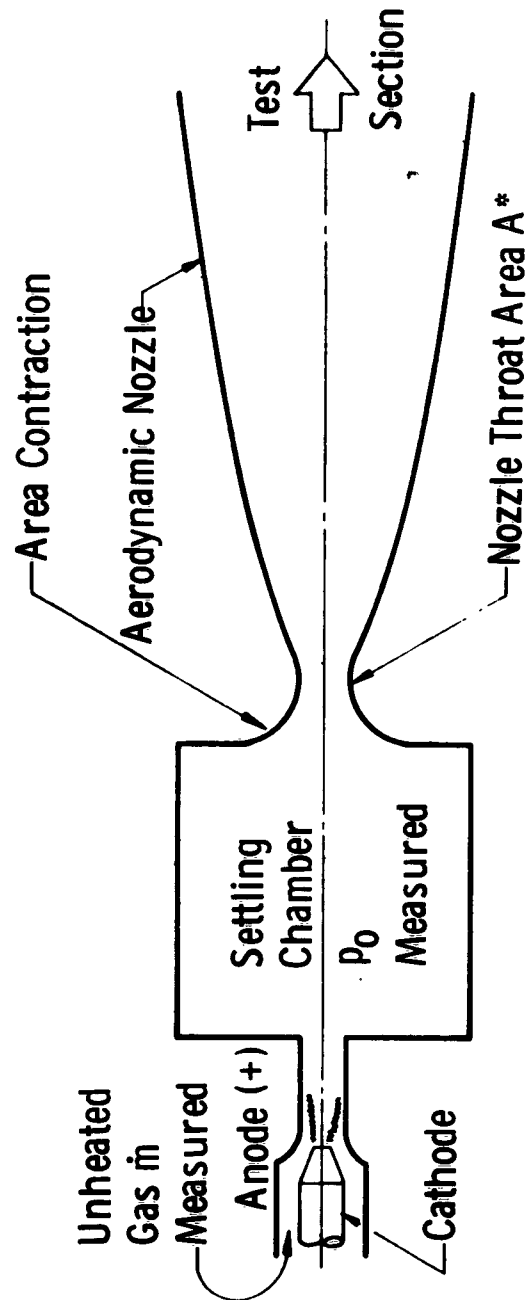


Fig. 1 Photograph of Gas Dynamic Wind Tunnel, Hypersonic (L) from the Operator's Side



Not to Scale

Fig. 2 Schematic Sketch of Arc-Heated Wind Tunnel

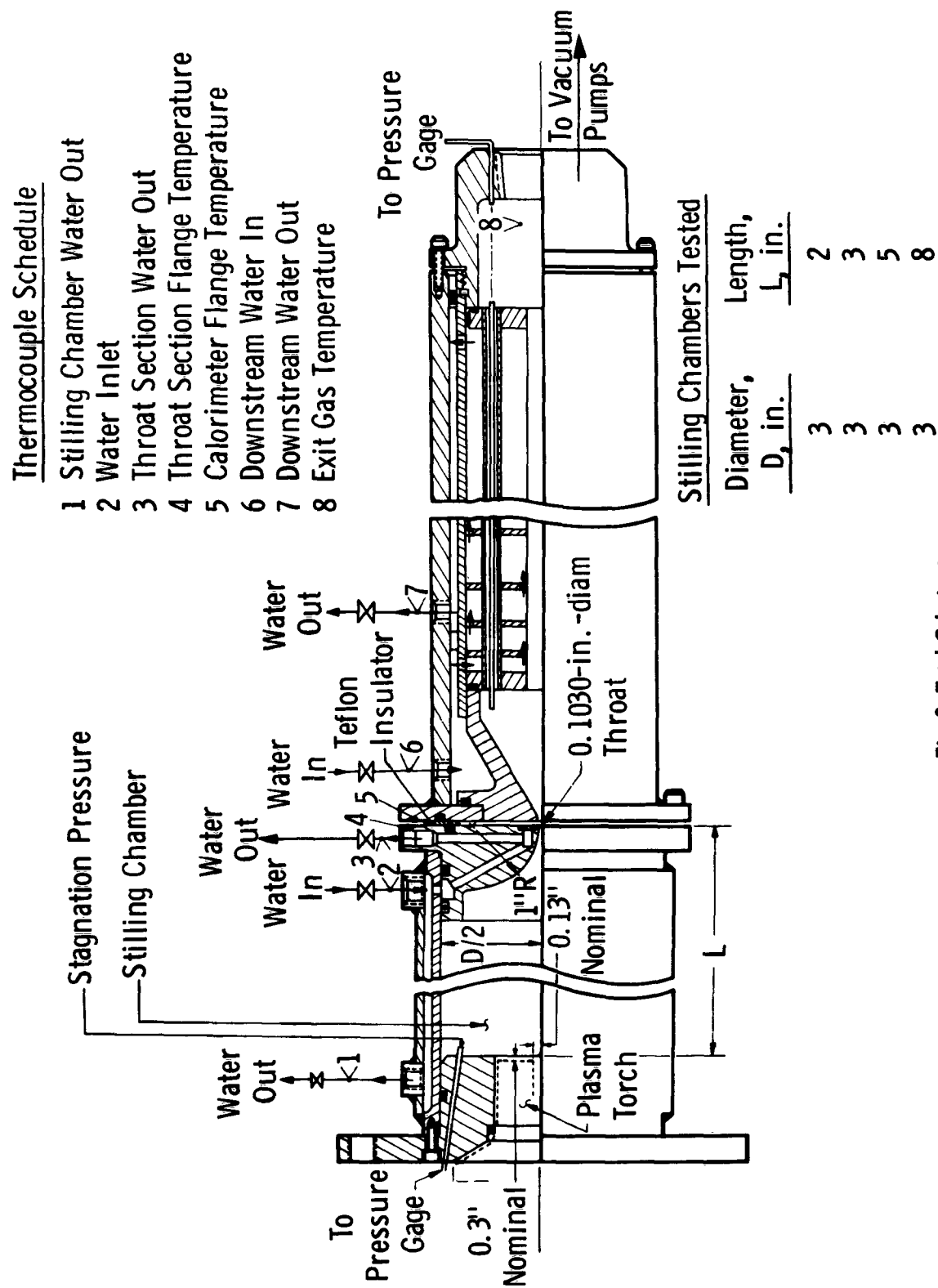


Fig. 3 Total Calorimeter

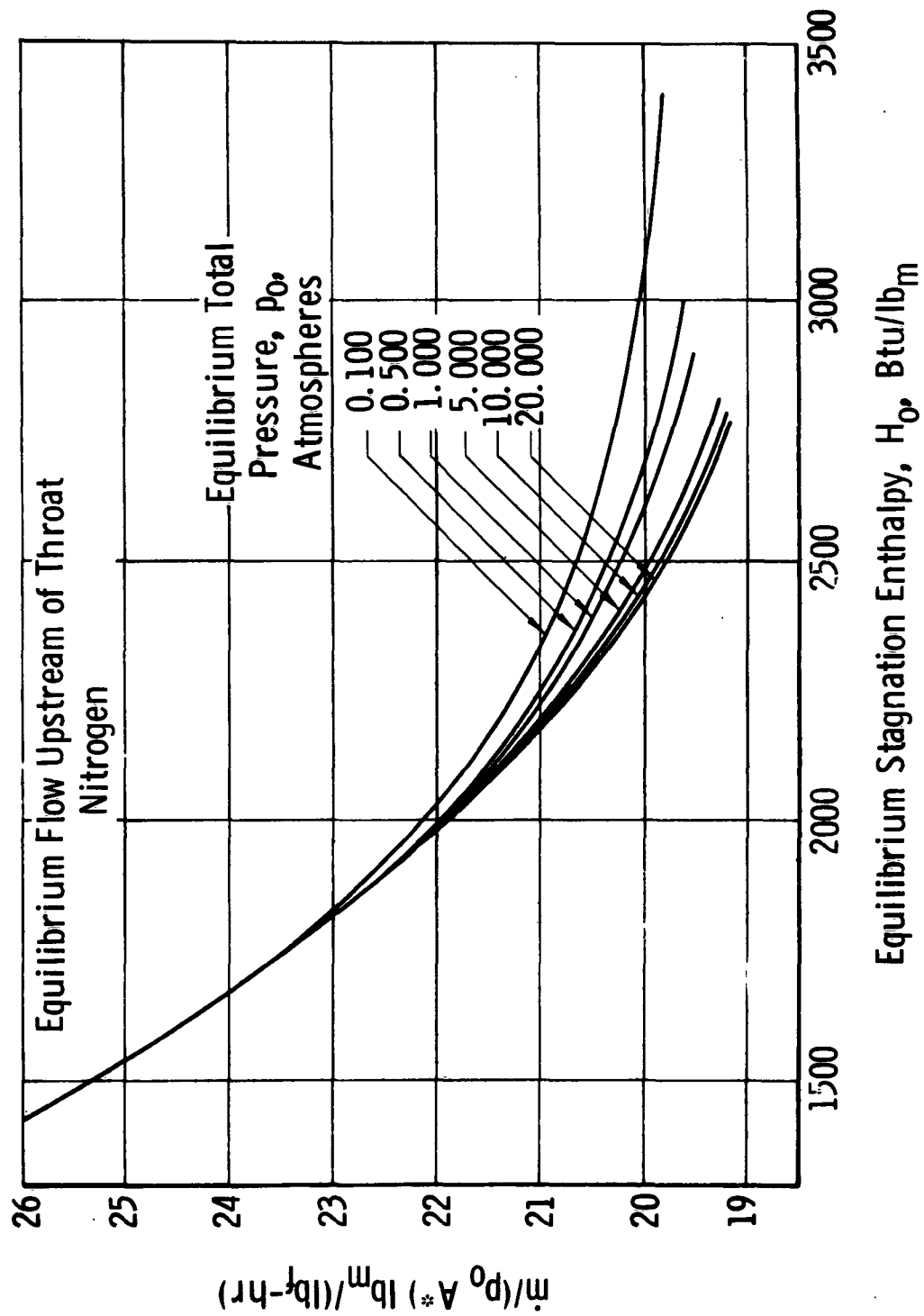


Fig. 4 Stagnation Enthalpy as a Function of  $\dot{m}$ ,  $P_0$ , and  $A^*$

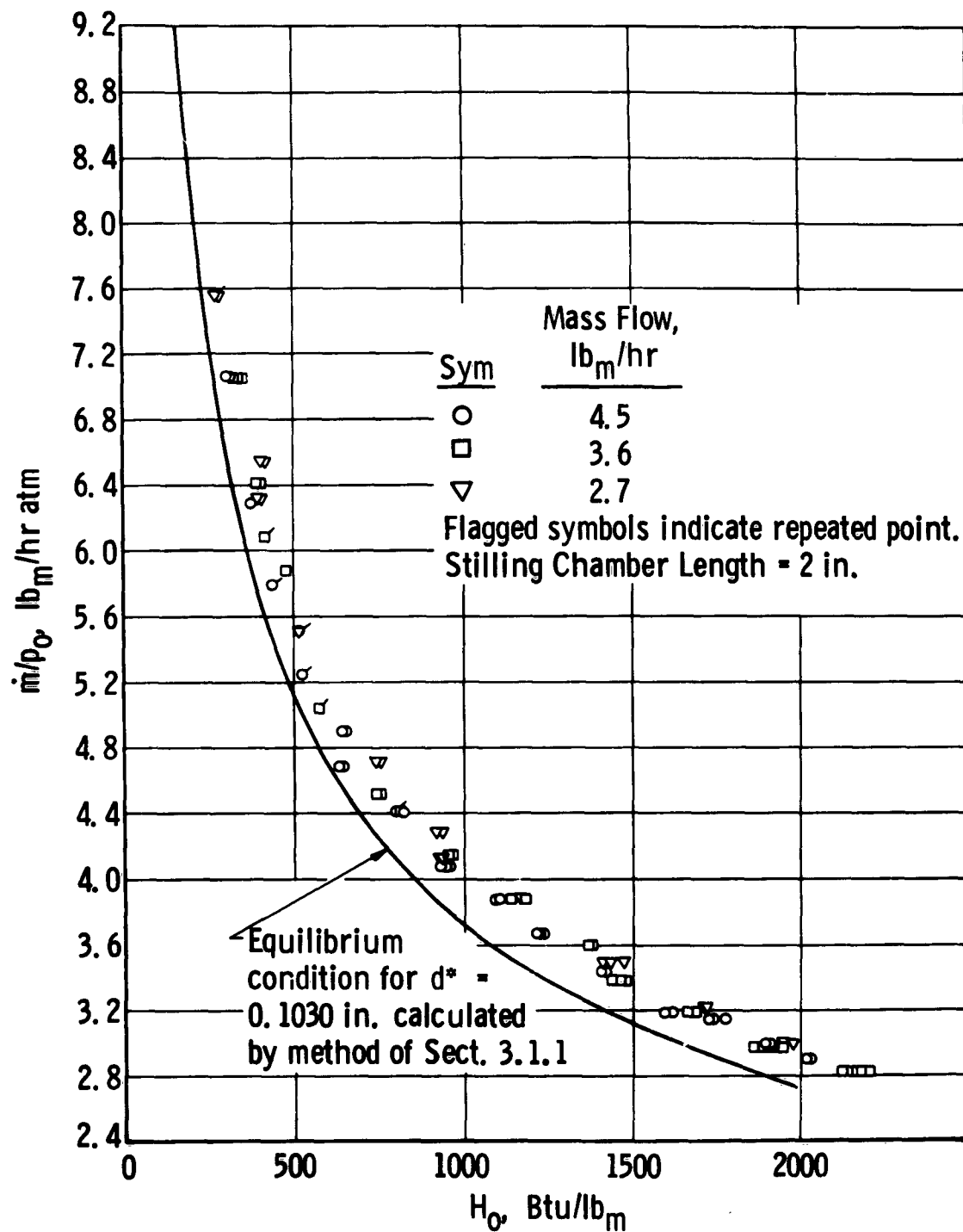


Fig. 5 Total Calorimeter Results for 2-in. Stilling Chamber

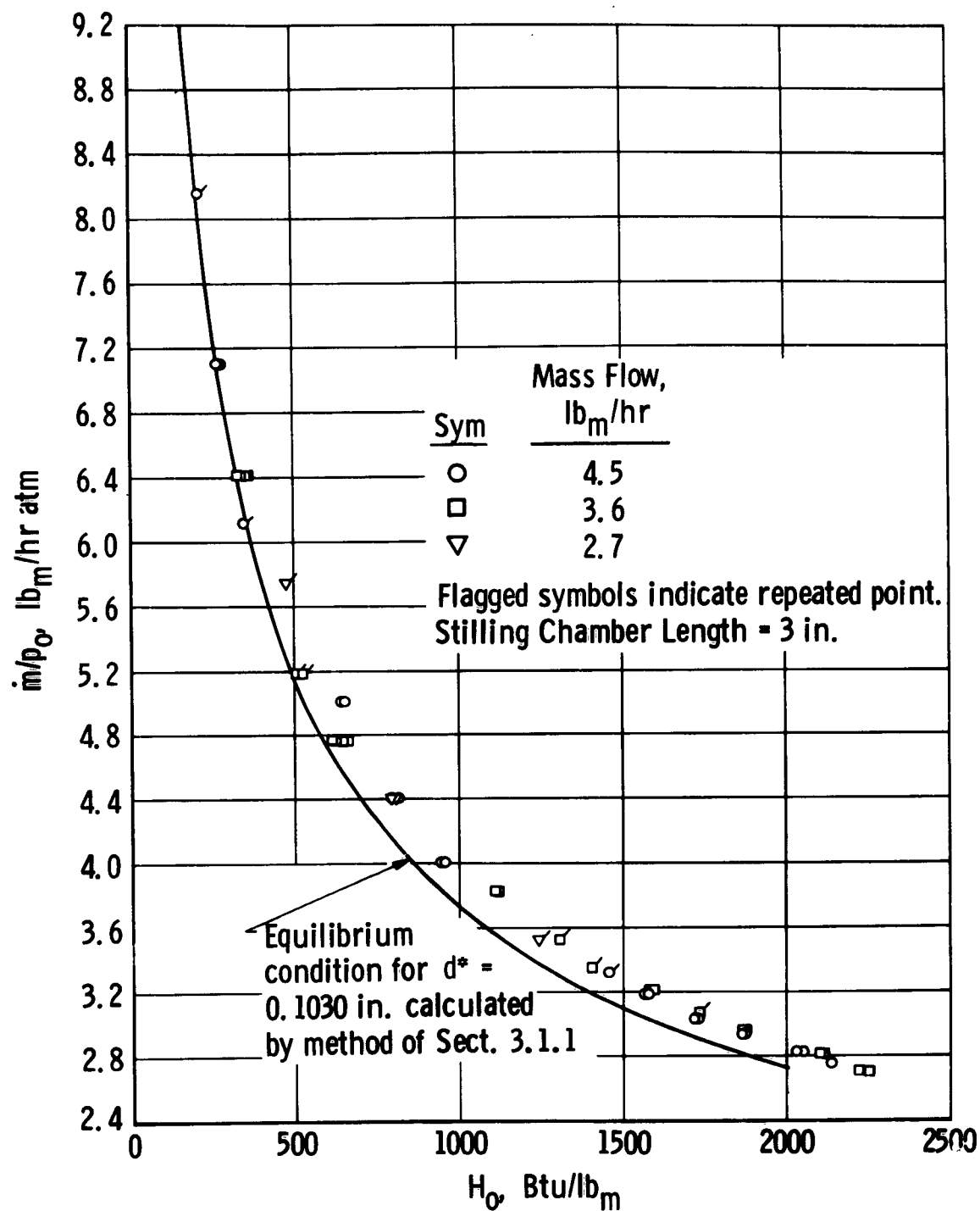


Fig. 6 Total Calorimeter Results for 3-in. Stilling Chamber

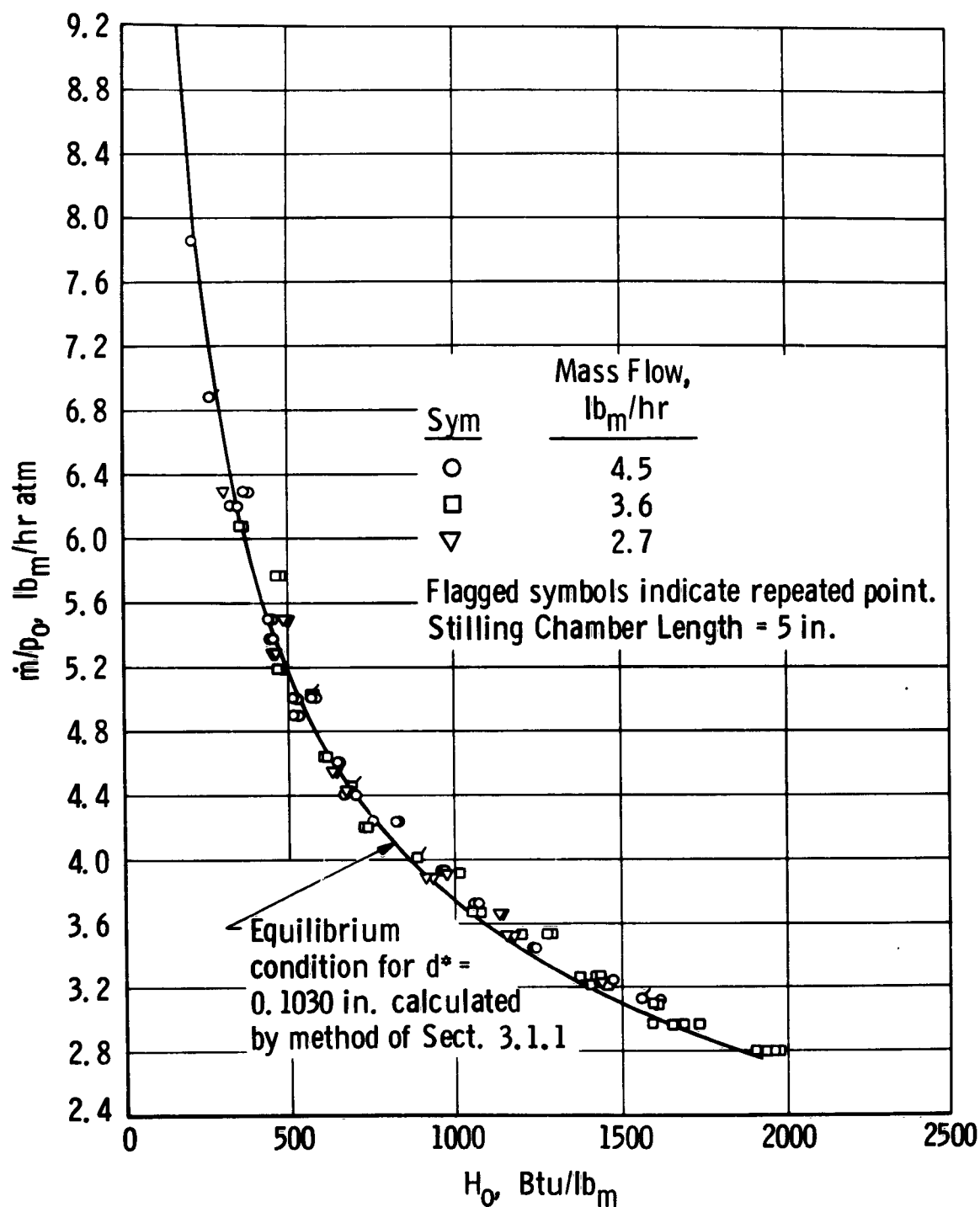


Fig. 7 Total Calorimeter Results for 5-in. Stilling Chamber



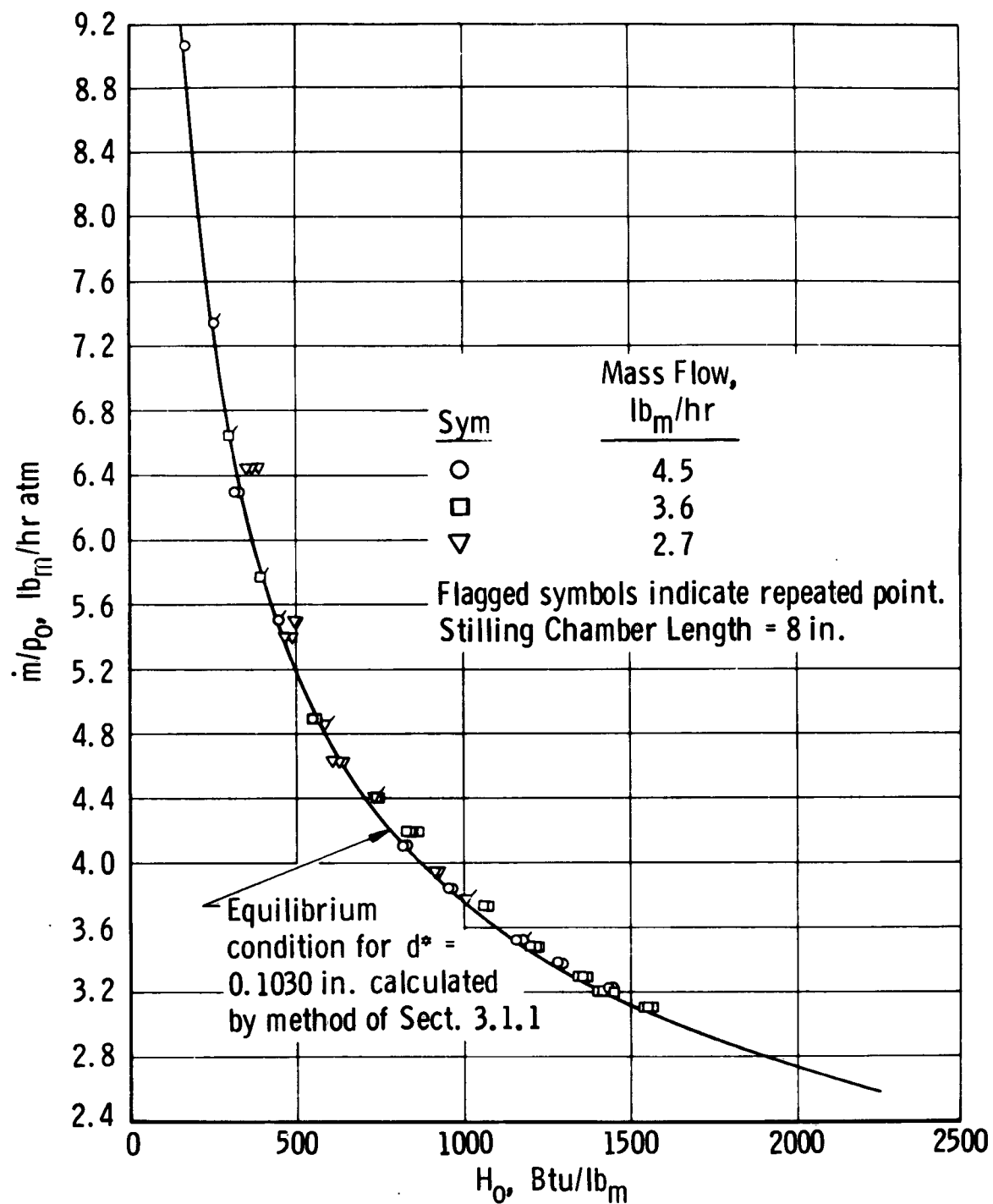


Fig. 8 Total Calorimeter Results for 8-in. Stilling Chamber

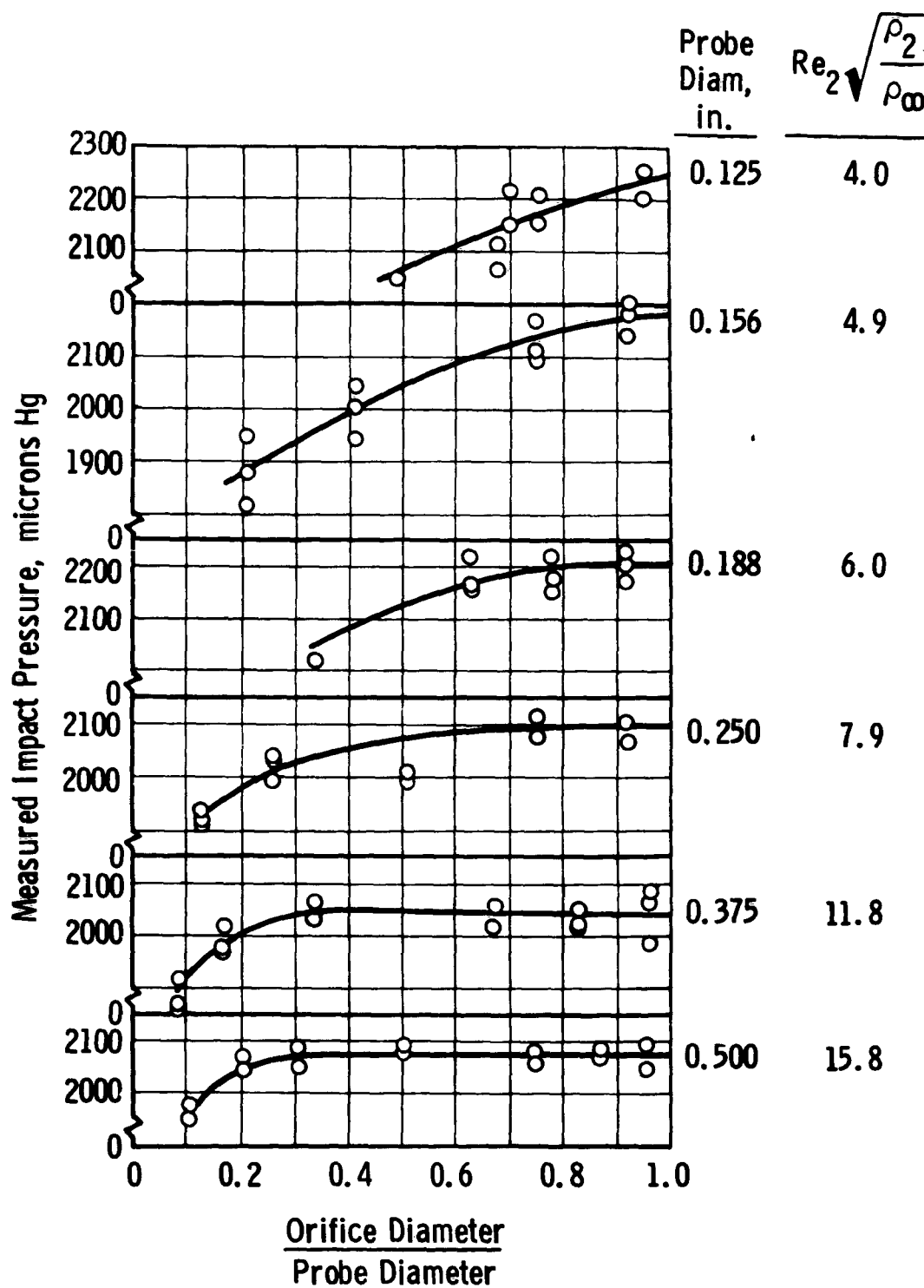


Fig. 9 Variation of Measured Impact Pressure with Orifice-to-Probe Diameter Ratio (Argon Gas, Reservoir Temperature  $\approx 7660^\circ\text{R}$ ,  $M_\infty = 8.2$ ,  $T_w/T_o \approx 0.19$ )

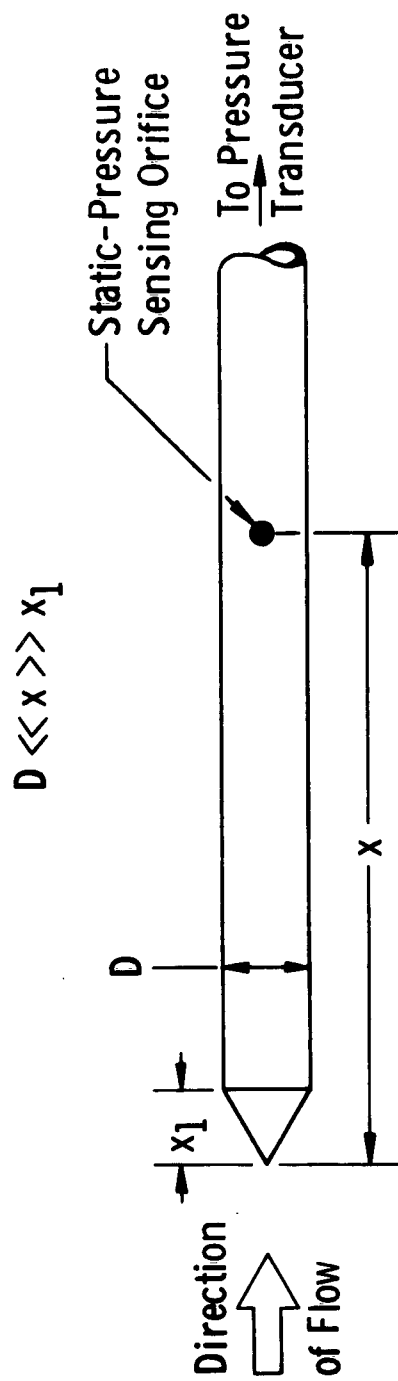


Fig. 10 Static-Pressure Probe

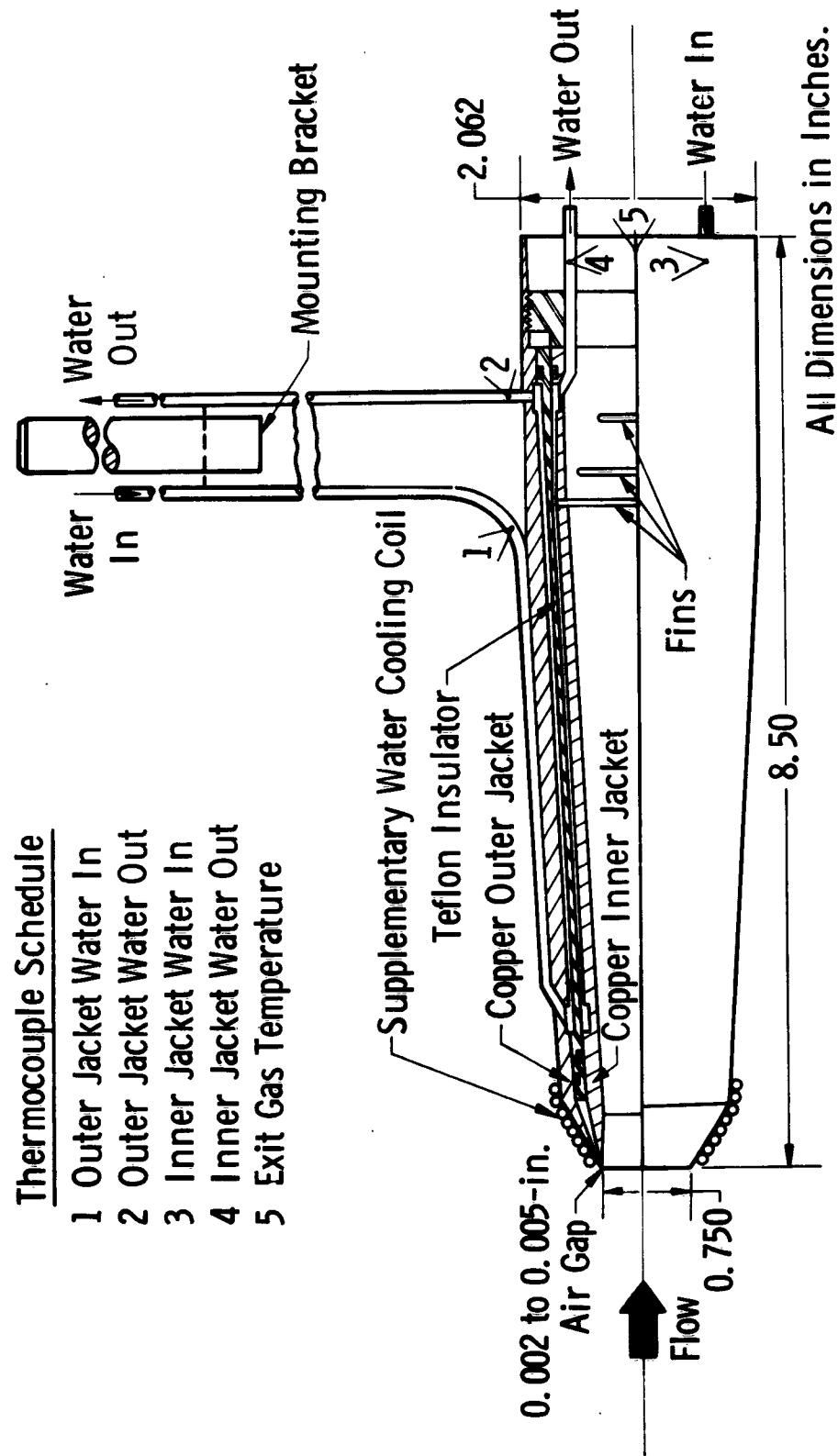


Fig. 11 Local Total-Enthalpy Probe

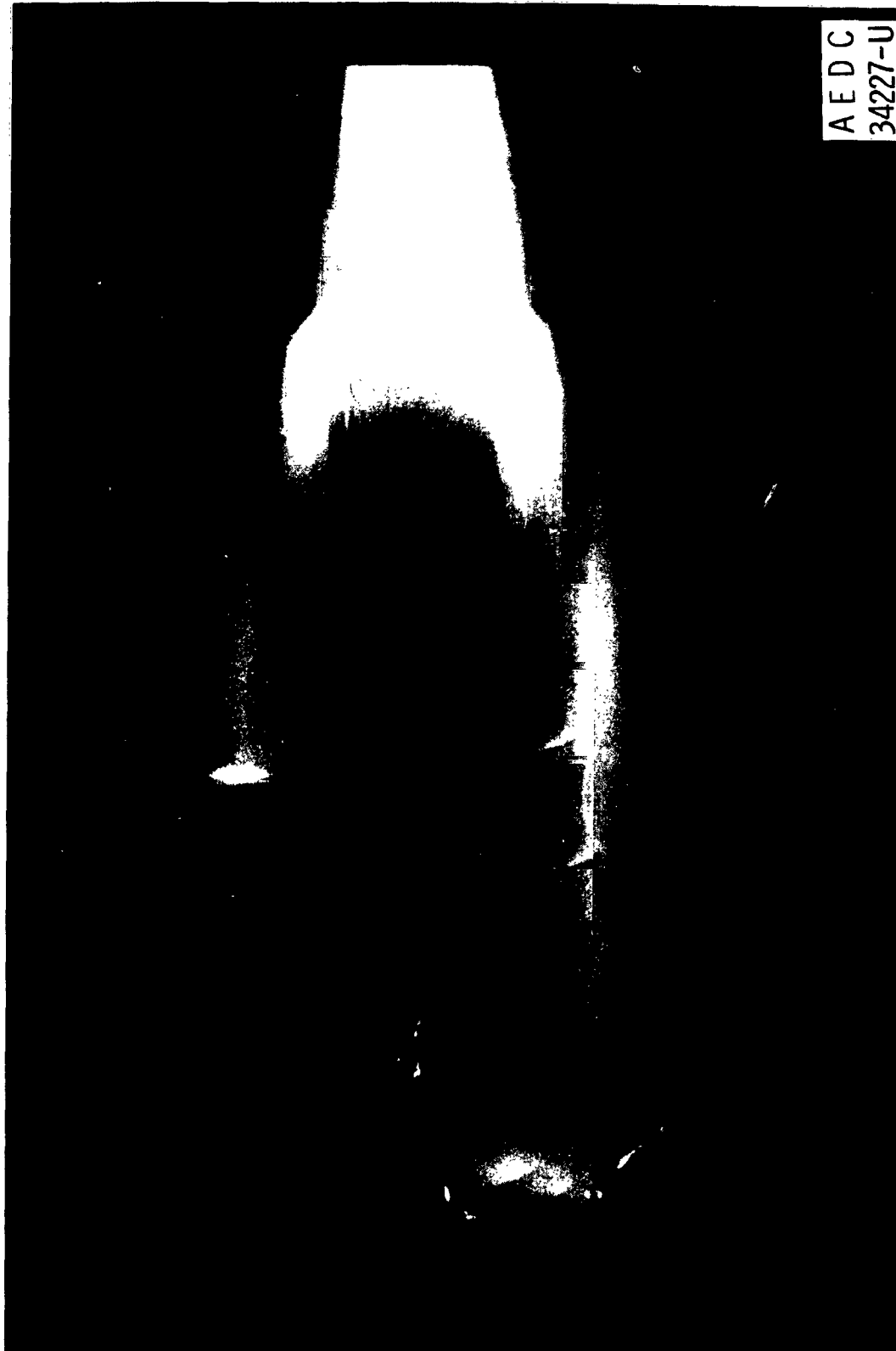


Fig. 12 Photograph of Local Total-Enthalpy Probe in Hypersonic Argon Flow

ARGON	
Sym	$T_0, ^\circ\text{R}$
○	5000
□	5535

$H_0$  computed is based on measured  $p_0$ ,  $\dot{m}$ ,  $A^*$ ,  $p_0'$  and assumed thermochemical flow process.

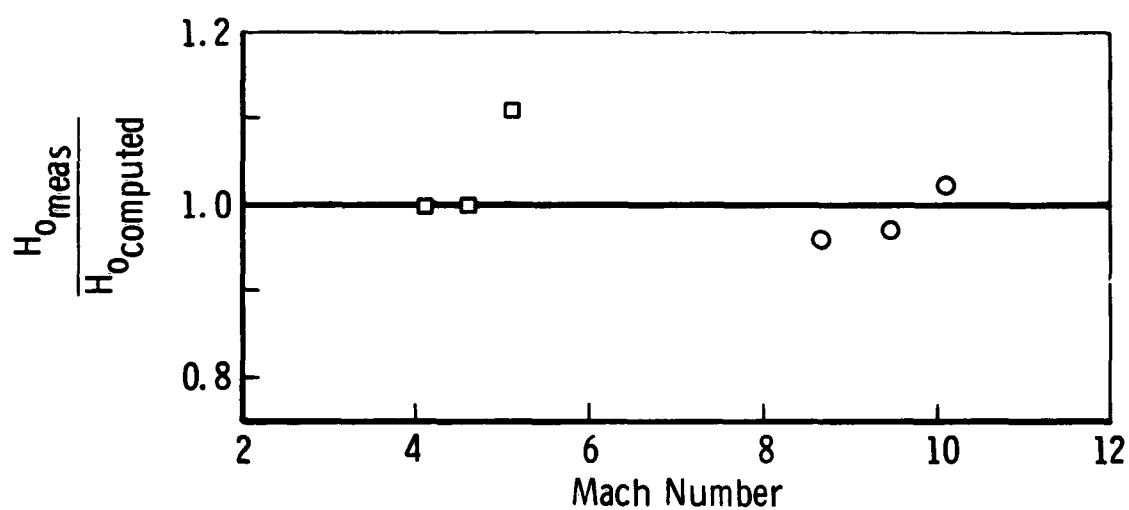


Fig. 13 Results from Local Total-Enthalpy Probe in the Low-Density, Arc-Heated Tunnel

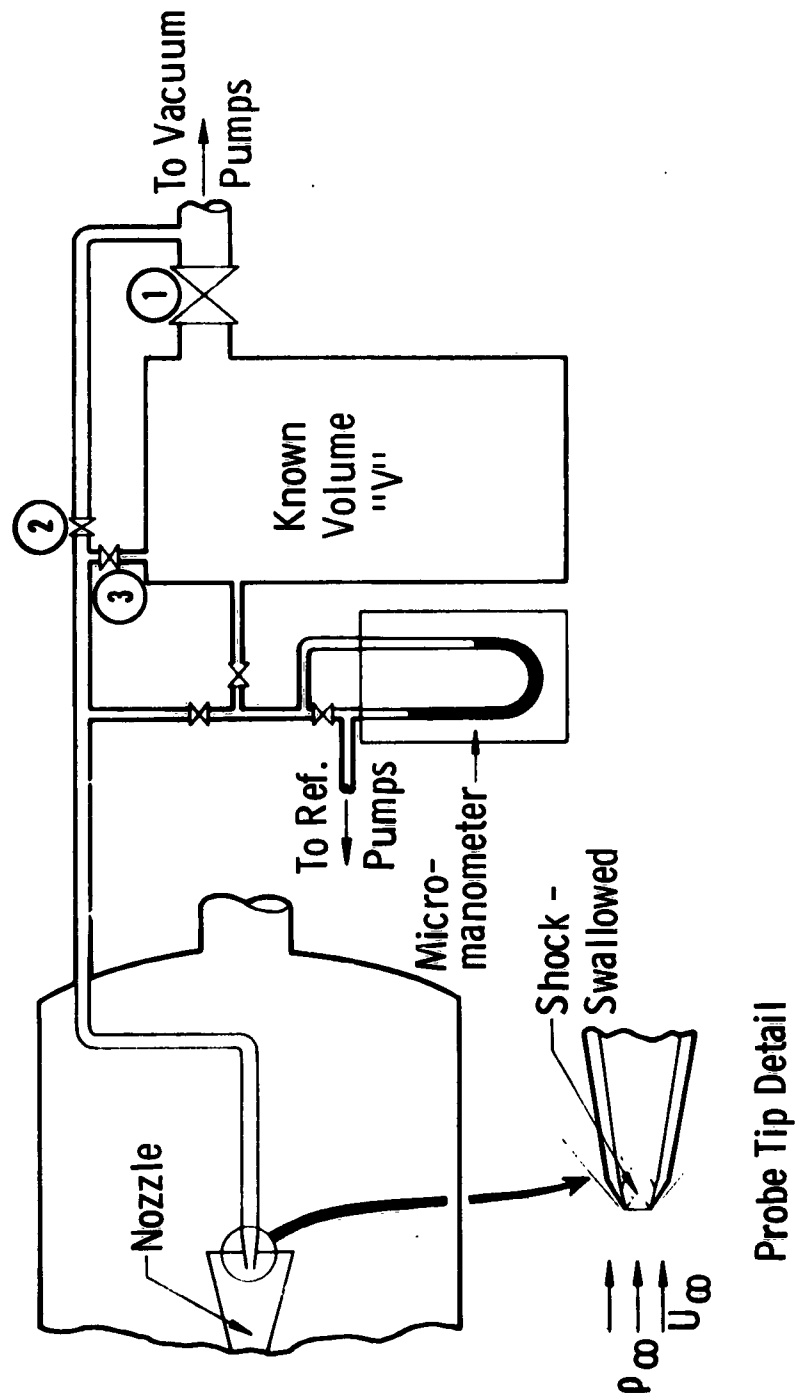


Fig. 14 Schematic Diagram of Mass-Flux Probe System

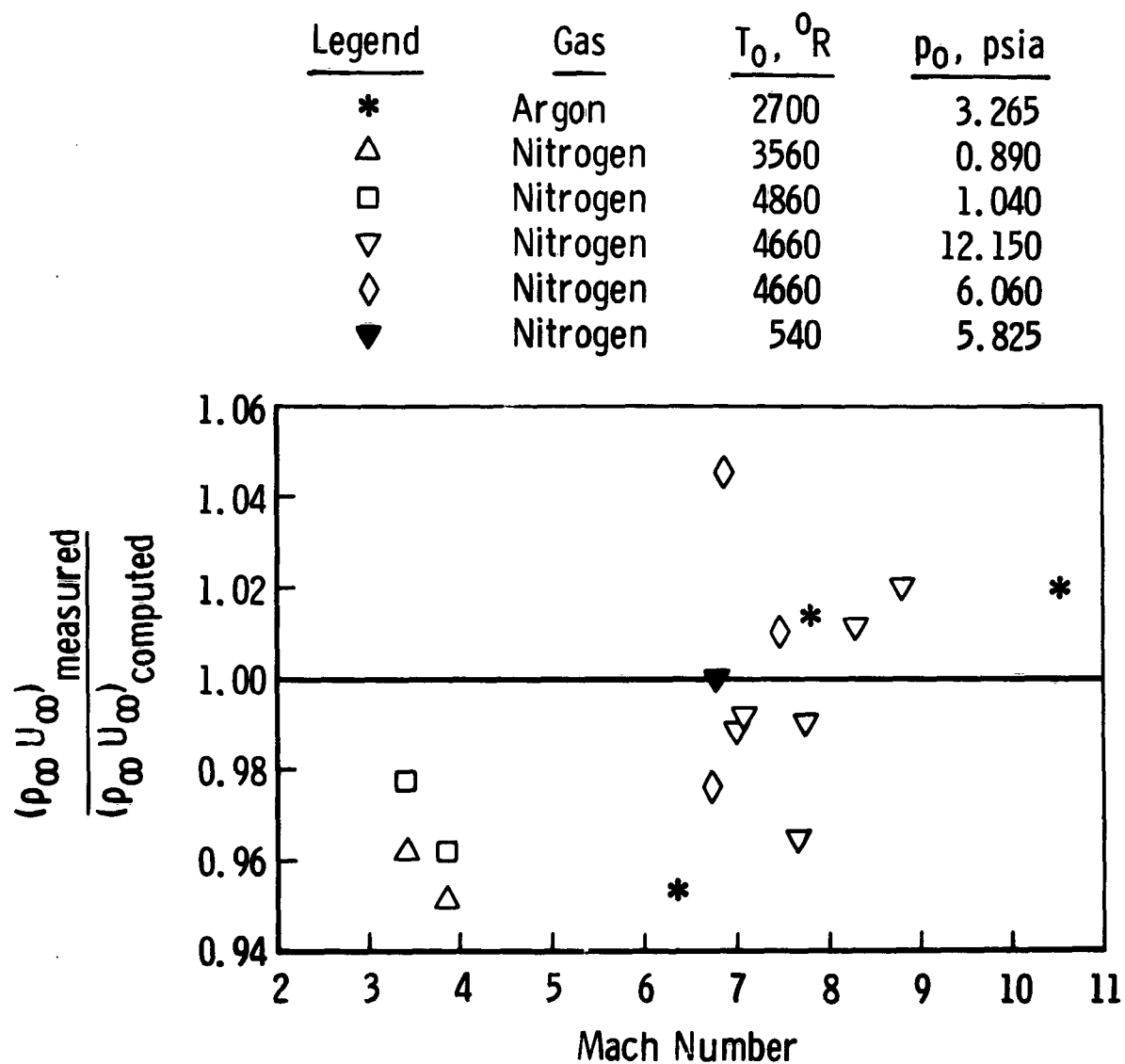


Fig. 15 Comparison of Measured and Calculated Local Mass Flux,  $\rho_\infty U_\infty$



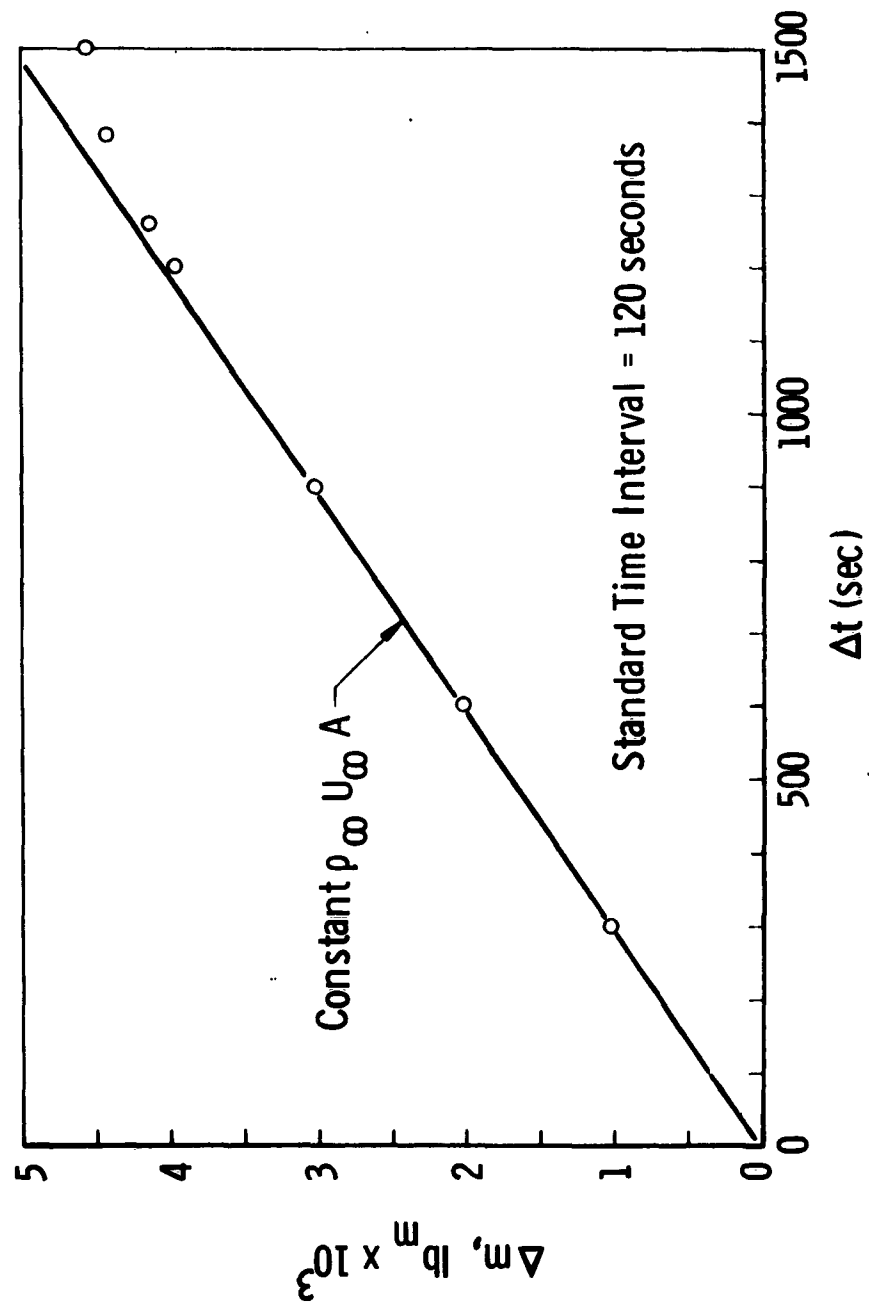


Fig. 16 Effect of Increased Time Interval on Measured Mass-Flux

## APPENDIX I

### PLASMA SWIRL

In some plasma torch configurations the working gas passes axially through the electrode region with no attempt to impose a tangential or swirl velocity component. This type of operation allows the arc to attach itself at some "preferred" location on the anode, possibly resulting in erosion of the anode in the region of attachment. It is often desirable to provide a means of rotating the arc so that the arc does not attach at one location but continuously moves around the anode. This may be accomplished by providing rotation by a magnetic field in the electrode region.

Another method of equalizing the heating is to introduce the gas to the electrode region with a tangential or swirl velocity component. The Thermal Dynamics Model U-50 plasma torch can be adapted to a gas swirl configuration with components available from the manufacturer.\* Such a configuration allows large increases of the power input to the torch.

It is conceivable that the use of swirl in the plasma torch could have a deleterious effect upon the flow properties in the wind tunnel test section, e.g., persistence of swirl into the test section. Because of the nature of the flow in the electrode section of the plasma torch, only a simple estimate of swirl velocity component is considered justified. When the so-called harsh swirl of the Thermal Dynamics U-50 torch is used, the gas is admitted to the electrode section through a number of small slots equally spaced around a circle of roughly 0.2-in. radius, concentric with the axes of the cathode and anode as shown in Fig. I-1. A crude calculation of tangential velocity entering the electrode section under conditions typical of the experiments discussed herein leads to an estimated 200 fps. This is only a few percent of any other velocities of interest throughout the tunnel, except for the settling chamber and near the stagnation point on a model.

A limited series of experiments has been carried out in an effort to learn the influence of swirl on the nozzle flow. In part, these experiments involved repetition of some of the diagnostic methods discussed in the preceding sections, but with the torch equipped to generate a gas swirl. In addition, two measurements not normally used for calibration were employed. These were selected to represent

---

\* Only the Thermal Dynamics "harsh swirl" is discussed herein.

typical experiments which may be conducted in a wind tunnel. Thus, the study of gas swirl was limited to the measurement of quantities which may reflect presence of swirl, rather than measurement of the swirl velocity component.

#### **STATIC-PRESSURE MEASUREMENTS**

The pressure probe shown in Fig. I-2 was tested in the wind tunnel test section with and without plasma swirl. This probe was designed to measure the static pressure on opposite sides of the probe behind the bow shock wave. It was anticipated that a swirl component of velocity in the test section would result in a pressure differential between the orifices as the probe was moved away from the flow centerline. Furthermore, this pressure difference would be expected to reverse itself as the probe moved across the axis of symmetry of the flow.

Over a cross section of the flow which included both a uniform core and a portion of the boundary layer, it was found that the average difference in pressure read with and without swirl was less than  $\pm 1$  percent. Thus, the results were practically identical for flow with and without plasma swirl, indicating that, within the ability to detect it by measurements of pressure, the swirl velocity component is not carried through to the test section of the low-density tunnel.

#### **HEAT-TRANSFER MEASUREMENTS**

Since many plasma-heated wind tunnels in existence today are used to study heat transfer to models, a comparison of the total heat-transfer rates to a hemispherical probe with and without plasma swirl is of some importance. This comparison was made in Tunnel L using a 0.25-in.-diam, hemispherical, water-cooled, calorimeter-type probe as sketched in Fig. I-3. With this probe the steady-state, total heat-transfer rate to the hemisphere is determined by measuring the linear temperature drop along a conductor of known thermal conductivity and cross-sectional area. The probe is calibrated by applying a known heat input.

For the plasma swirl configuration, the heat-transfer rates were about 7 percent higher than the data obtained with the normal configuration. The explanation of this result rests on data presented in following sections.

## IMPACT-PRESSURE MEASUREMENTS

Since impact-pressure measurements are of primary concern in the flow calibration of most wind tunnels, a comparison of measured impact-pressure profiles in the test section with and without plasma swirl is also of importance. Radial surveys were made at several axial stations along the nozzle.

Although the general appearance of the impact-pressure surveys was quite similar with and without swirl, the magnitudes of the measured impact pressures were about 3 percent higher with the plasma swirl configuration. This small but consistent difference was seen in all impact-pressure surveys which were made.

## TOTAL CALORIMETER MEASUREMENTS

The total calorimeter measurements described in Section 3.1.2 were obtained with the normal plasma torch configurations. The calorimeter was operated at two settling chamber lengths with the plasma swirl configuration to obtain comparable data. The results are presented in Fig. 1-4 for the 2- and 5-in. settling chamber lengths in combination with a 0.1-in. -diam nozzle throat. Part of the earlier results are also presented in the figure for comparison.

For the 2-in. chamber, the total enthalpy with plasma swirl is in excellent agreement with the previous data. For the 5-in. stilling chamber, the agreement is good, although it does appear that the total-enthalpy measurements with swirl are about 6 percent higher than the no-swirl data. The comparison is made more difficult because the torch will not readily operate at the lower power levels with plasma swirl.

Total calorimeter results obtained at lower stilling chamber pressures are more susceptible to a departure from equilibrium since the number of collisions may not be great enough for complete recombination of dissociated molecules to occur. In order to show more positively any such departure from equilibrium or mixing uniformity which might result from the gas swirl configuration, the total calorimeter was run at total pressures on the order of 0.1 to 0.5 atm with and without plasma swirl. This was accomplished by replacing the nominal 0.1-in. throat of the aerodynamic nozzle with a nominal 0.25-in. -diam throat. Thus, the area-contraction ratio was decreased by a factor of 6.25 when the larger throat was installed.

These results are presented in Fig. I-5. In all cases, the measured total enthalpy is significantly greater than that predicted by the theoretical consideration given in Section 3.1.1. The explanation for this difference may well be a lesser degree of equilibrium and uniformity of the flow at the nozzle entrance when swirling gas is admitted to the electron section.

It is of interest to compare the "efficiency" of the gas swirl configuration with that of the normal configuration. The tunnel efficiency is defined as the ratio of total enthalpy of the flow passing through the aerodynamic throat to the electrical power supplied to the plasma torch. The torch efficiency is found by adding to the flow enthalpy all of the losses measured downstream of the plasma torch and dividing by the input electrical power.

These two efficiencies are presented in Fig. I-6a for typical flow conditions with the nominal 0.25-in. throat. The plasma swirl configuration demonstrates a significantly higher torch efficiency and tunnel efficiency than does the normal configuration. It must be remembered that these flow conditions exhibited an apparent lack of equilibrium and/or uniformity of flow at the nozzle entrance. Thus, they have not been used in normal tunnel operations.

Another efficiency comparison can be made for the customary flow conditions where equilibrium and uniformity of flow have been shown to be essentially complete upstream of the nozzle throat. Such conditions are obtained with the nominal 0.1-in. throat, where the total pressure is on the order of one atmosphere. The tunnel efficiency and torch efficiency are shown in Fig. I-6b for these flow conditions, with and without plasma swirl. The normal configuration data were obtained with an anode orifice diameter of 0.25 in., known from earlier experiments to be the optimum size. The data from both configurations are in close agreement, indicating that the plasma swirl configuration has the same efficiency as the optimum normal configuration under these flow conditions.

#### **CONCLUSIONS REGARDING PLASMA SWIRL**

No evidence was found to indicate the presence of swirl in the test section. Some evidence was found to indicate that the flow process taking place in the settling chamber and nozzle was changed by plasma swirl, and that these changes could have varying degrees of influence on the test section flow properties.

The evidence of slightly higher heat-transfer rate to a model in the test section with plasma swirl is consistent with the observation of a slightly higher total enthalpy and impact pressure when swirl was used. The heat-transfer rates calculated by appropriate theory for the two cases reveal that the increased rate when swirl was used is almost exactly predicted on the basis of the higher  $H_0$  and  $p_i$  values measured. Thus, the higher heating rate apparently resulted from changed flow in the settling section and aerodynamic nozzle, with changes in the settling section being the dominant factor. In other words, there was no evidence of an influence of swirl, per se, in the test section after the settling section conditions were accounted for.

It is important to bear in mind the particular conditions of this experiment. Specifically, (1) a relatively large settling section was used, (2) a particular type and degree of swirl was imparted, and (3) the actual decay of the swirl was not traced under widely varying conditions. Only the latter type of measurement would provide completely general results. However, it is apparent that swirl may be used without compromising test section flow quality if the swirl is imparted in a well-controlled, uniform manner, in relatively small degree, if a relatively large settling chamber is located downstream of the arc heater, and if a high area-contraction ratio characterizes the entrance to the aerodynamic nozzle.

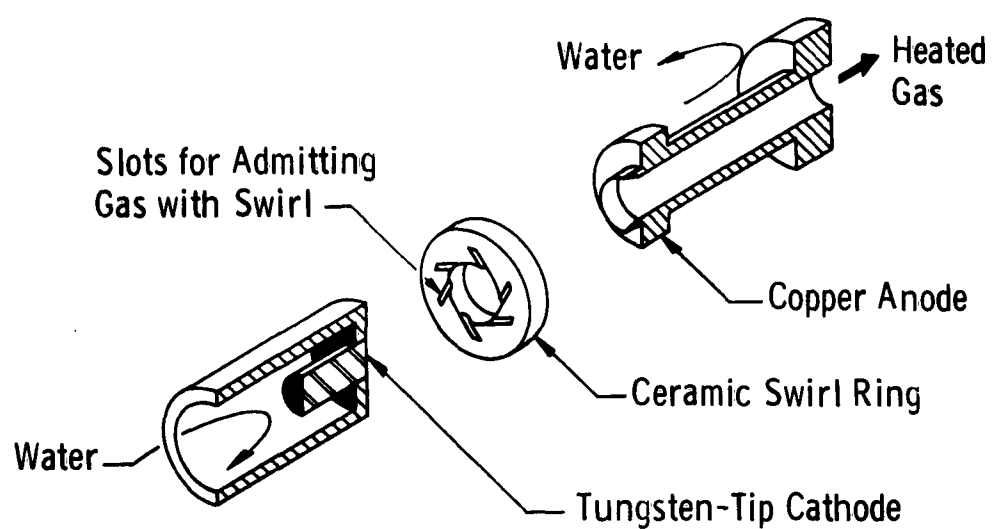


Fig. 1-1 Electrode Configuration with Plasma Swirl

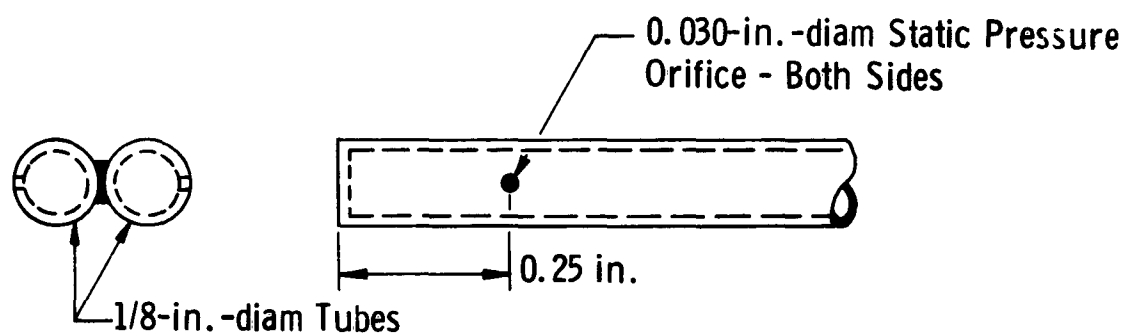


Fig. 1-2 Special Static-Pressure Probe

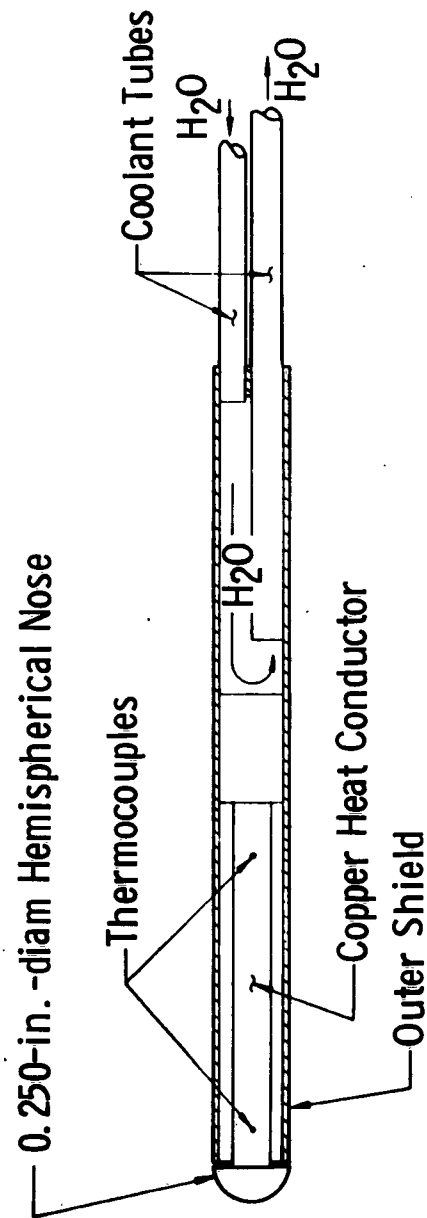
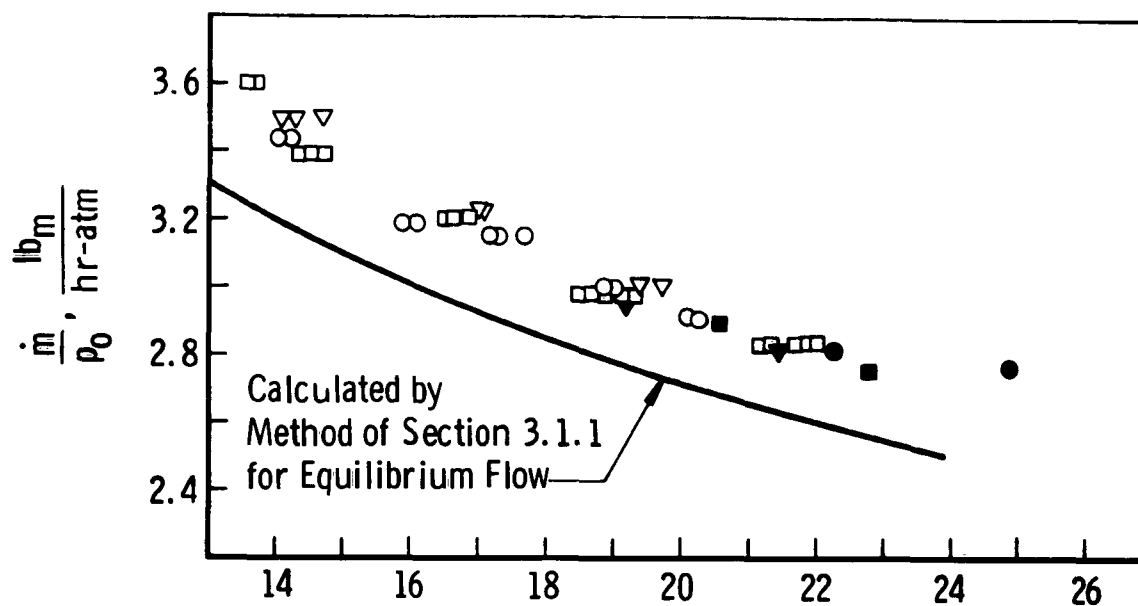


Fig. 1-3 Water-Cooled Heat-Transfer Probe

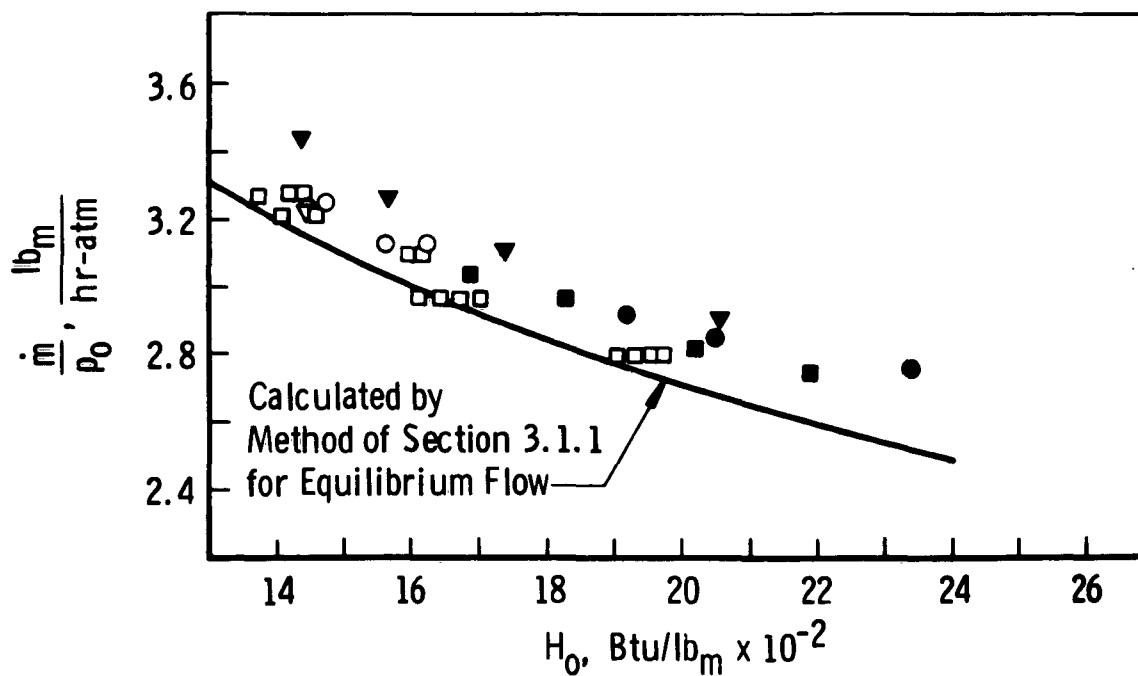


○ 4.5 lb<sub>m</sub>/hr□ 3.6 lb<sub>m</sub>/hr▽ 2.7 lb<sub>m</sub>/hr

Solid Symbols Indicate Swirl



a. Nominal 2-in. Stilling Chamber Length



b. Nominal 5-in. Stilling Chamber Length

Fig. 1-4 Measured Enthalpy with and without Swirl for  $d^* = 0.103$  in.

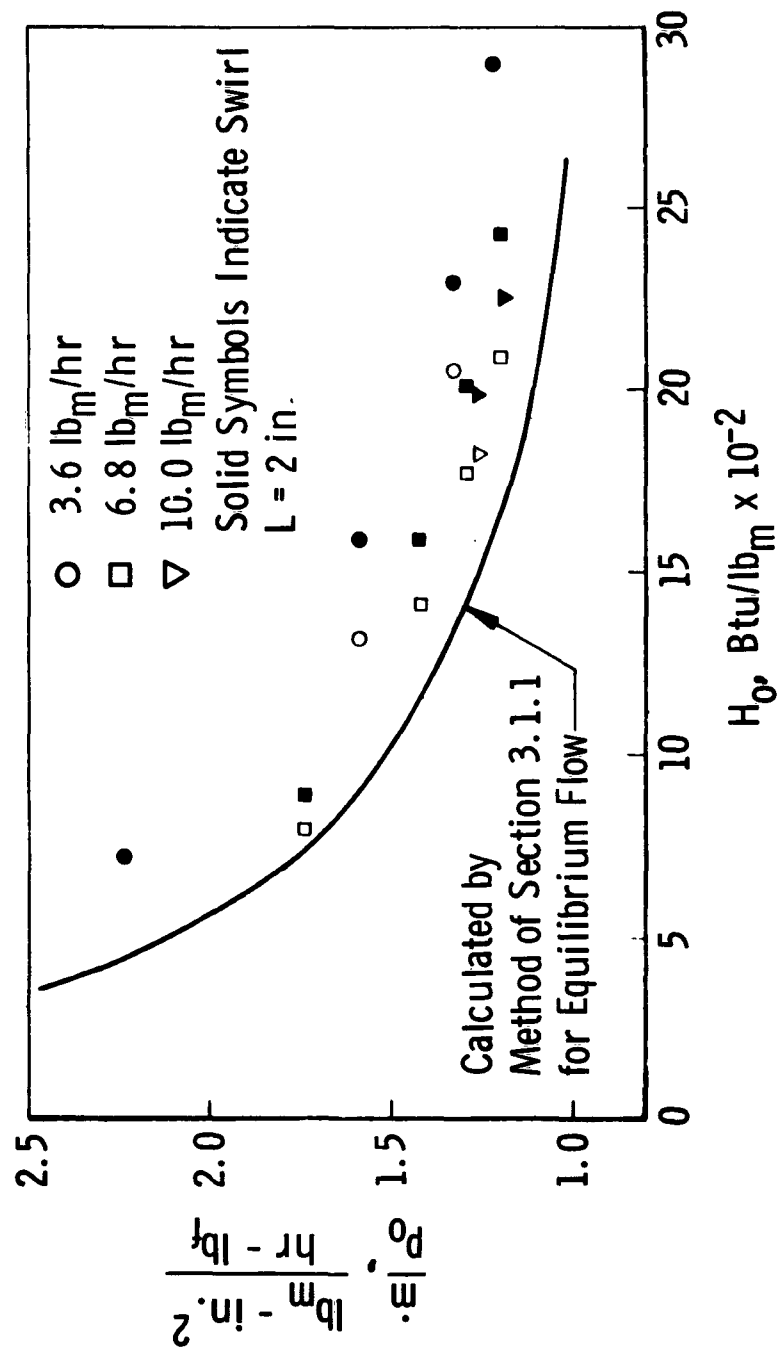


Fig. 1-5 Measured Enthalpy with and without Swirl for  $d^* = 0.252$  in.

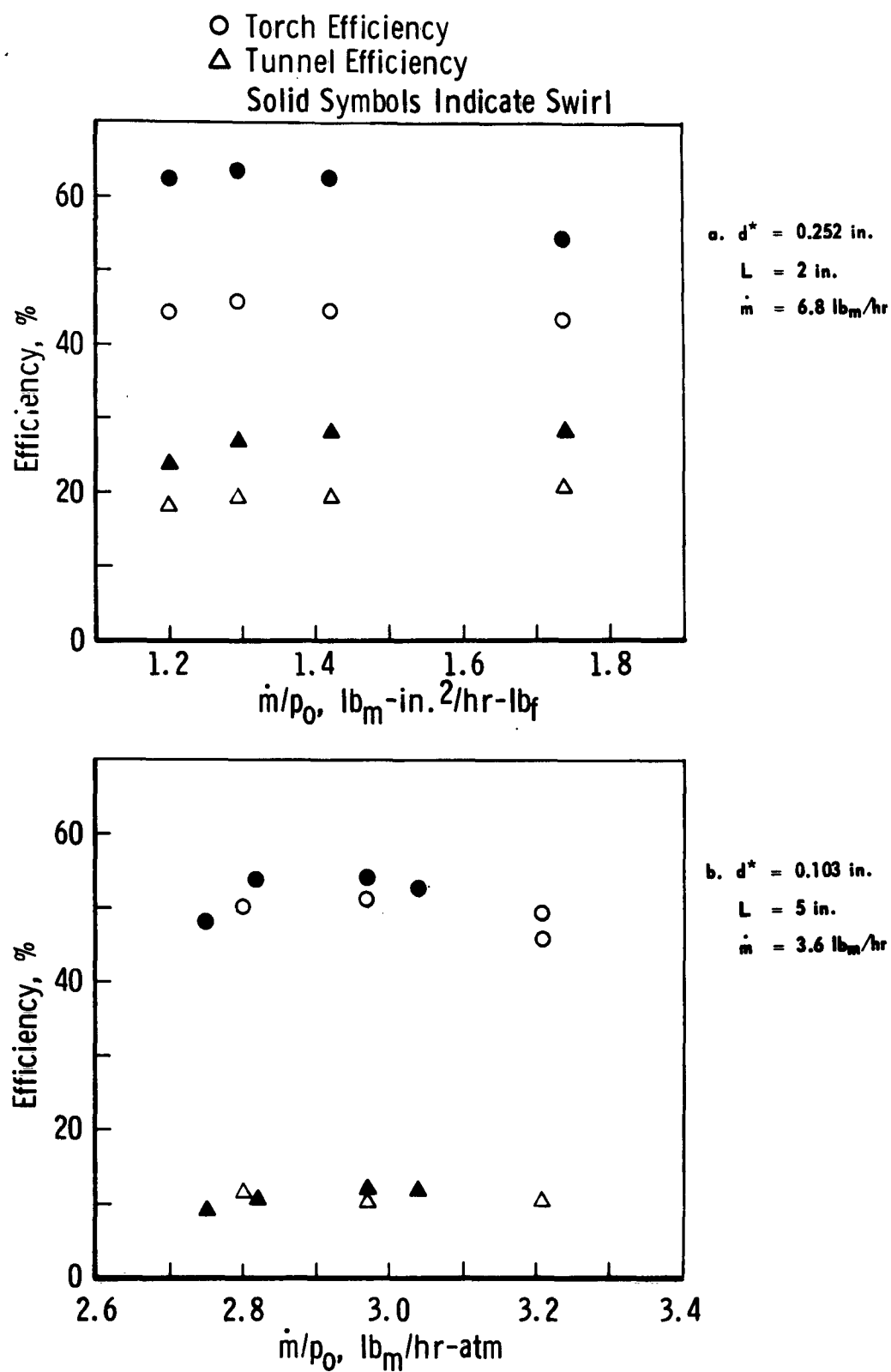


Fig. 1-6 Torch and Tunnel Efficiency with and without Swirl